Improvements to a MODIS Global Terrestrial Evapotranspiration Algorithm

Article *in* Remote Sensing of Environment · August 2011
DOI: 10.1016/j.rse.2011.02.019

3 authors, including:

Qiaozhen Mu
Science Systems and Applications, Inc.
78 PUBLICATIONS **4,688** CITATIONS

SEE PROFILE

Remote Sensing of Environment 115 (2011) 1781–1800

Contents lists available at ScienceDirect

Remote Sensing of Environment

journal homepage: www.elsevier.com/locate/rse

Improvements to a MODIS global terrestrial evapotranspiration algorithm

Qiaozhen Mu *, Maosheng Zhao, Steven W. Running

Numerical Terradynamic Simulation Group, Department of Ecosystem and Conservation Sciences, The University of Montana, Missoula, MT 59812, USA

ARTICLE INFO

Article history:
Received 7 October 2010
Received in revised form 25 February 2011
Accepted 27 February 2011
Available online 8 April 2011

Keywords:
Evapotranspiration
Stomatal conductance
Soil surface evaporation
Vegetation cover fraction
MODIS

ABSTRACT

MODIS global evapotranspiration (ET) products by Mu et al. [Mu, Q., Heinsch, F. A., Zhao, M., Running, S. W. (2007). Development of a global evapotranspiration algorithm based on MODIS and global meteorology data. Remote Sensing of Environment, 111, 519–536. doi: 10.1016/j.rse.2007.04.015] are the first regular 1-km^2 land surface ET dataset for the 109.03 Million km^2 global vegetated land areas at an 8-day interval. In this study, we have further improved the ET algorithm in Mu et al. (2007a, hereafter called old algorithm) by 1) simplifying the calculation of vegetation cover fraction; 2) calculating ET as the sum of daytime and nighttime components; 3) adding soil heat flux calculation; 4) improving estimates of stomatal conductance, aerodynamic resistance and boundary layer resistance; 5) separating dry canopy surface from the wet; and 6) dividing soil surface into saturated wet surface and moist surface. We compared the improved algorithm with the old one both globally and locally at 46 eddy flux towers. The global annual total ET over the vegetated land surface is 62.8×10^3 km^3, agrees very well with other reported estimates of 65.5×10^3 km^3 over the terrestrial land surface, which is much higher than 45.8×10^3 km^3 estimated with the old algorithm. For ET evaluation at eddy flux towers, the improved algorithm reduces mean absolute bias (MAE) of daily ET from 0.39 mm day^{-1} to 0.33 mm day^{-1} driven by tower meteorological data, and from 0.40 mm day^{-1} to 0.31 mm day^{-1} driven by GMAO data, a global meteorological reanalysis dataset. MAE values by the improved ET algorithm are 24.6% and 24.1% of the ET measured from towers, within the range (10–30%) of the reported uncertainties in ET measurements, implying an enhanced accuracy of the improved algorithm. Compared to the old algorithm, the improved algorithm increases the skill score with tower-driven ET estimates from 0.50 to 0.55, and from 0.46 to 0.53 with GMAO-driven ET. Based on these results, the improved ET algorithm has a better performance in generating global ET data products, providing critical information on global terrestrial water and energy cycles and environmental changes.

1. Introduction

All organisms require water for their survival (Oki & Kanae, 2006). Unlike most other natural resources, water circulates and forms closed hydrological cycles. The terrestrial water cycle is of critical importance to a wide array of Earth system processes. It plays a central role in climate and meteorology, plant community dynamics, and carbon and nutrient biogeochemistry (Vörösmarty et al., 1998; Zhao & Running, 2010). Demand for the world's increasingly scarce water supply is rising rapidly, challenging its availability for food production and putting global food security at risk. Agriculture, upon which a burgeoning population depends for food, is competing with industrial, household, and environmental uses for this scarce water supply (Rosegrant et al., 2003; Vörösmarty et al., 2010). The water withdrawals from the renewable freshwater resources include blue water from the surface and groundwater as water resources, and green water from the beneficial evapotranspiration (ET) as a loss from the precipitated water over non-irrigated croplands (Oki & Kanae, 2006). Global climate change will affect precipitation and ET, and hence influence the renewable freshwater resources. ET is the second largest component (after precipitation) of the terrestrial water cycle at the global scale, since ET returns more than 60% of precipitation on land back to the atmosphere (Korzoun et al., 1978; L'vovich & White, 1990) and thereby conveys an important constraint on water availability at the land surface. In addition, ET is an important energy flux since land ET uses up more than half of the total solar energy absorbed by land surfaces (Trenberth et al., 2009). Accurate estimation of ET not only meets the growing competition for the limited water supplies and the need to reduce the cost of the irrigation projects, but also it is essential to projecting potential changes in the global hydrological cycle under different climate change scenarios (Teuling et al., 2009).

Remote sensing has long been recognized as the most feasible means to provide spatially distributed regional ET information on land surface. Remotely sensed data, especially those from polar-orbiting satellites, provide temporally and spatially continuous information

* Corresponding author. Tel.: +1 406 243 6218; fax: +1 406 243 4510.
E-mail addresses: qiaozhen@ntsg.umt.edu (Q. Mu), zhao@ntsg.umt.edu (M. Zhao), swr@ntsg.umt.edu (S.W. Running).

0034-4257/$ – see front matter © 2011 Elsevier Inc. All rights reserved.
doi:10.1016/j.rse.2011.02.019

over vegetated surfaces useful for regional measurement and monitoring of surface biophysical variables affecting ET, including albedo, biome type and leaf area index (LAI) (Los et al., 2000). The MODerate Resolution Imaging Spectroradiometer (MODIS) onboard NASA's Terra and Aqua satellites, provide unprecedented information regarding vegetation and surface energy (Justice et al., 2002), which can be used for regional and global scale ET estimation in near real-time. Three types of methods have been developed to estimate ET from remote sensing data: (1) empirical/statistical methods which link measured ET or estimated ET to large scales with remotely sensed vegetation indices (Glenn, Huete, et al., 2008a; Glenn, Morino, et al., 2008b; Jung et al., 2010; Nagler et al., 2005); (2) physical models that calculate ET as the residual of surface energy balance (SEB) through remotely sensed thermal infrared data (Allen et al., 2007; Bastiaanssen et al., 2005; Kustas & Anderson, 2009; Overgaard et al., 2006); (3) and other physical models such as using the Penman–Monteith logic (Monteith, 1965) to calculate ET (Cleugh et al., 2007; Mu et al., 2007a). We only describe the physical models in this article since we focus on the dynamics of ET process.

For SEB-based physical ET models, thermal-IR based land surface temperature (LST) is a critical remote sensing variable used in these satellite based SEB models (Bastiaanssen et al., 1998a; Bastiaanssen et al., 1998b; Nishida et al., 2003; Su, 2002), yet there are some disadvantages when applying LST to ET estimations at the global scale. Firstly, Hope et al. (2005) found that the relationship between thermal-IR based LST and NDVI at high-latitudes is opposite to that of mid-latitude regions because arctic tundra ecosystems characterized by permafrost provide a large sink for energy below the ground surface. Secondly, sensible heat flux (H) is estimated using the aerodynamic surface–air temperature gradient (or combination of gradients) and aerodynamic resistance, where generally LST has been used as a surrogate for aerodynamic temperature, which is the main reason that accurate estimates of H are very difficult to achieve (Gowda et al., 2008). Thirdly, among other complications, ET can often exceed net incoming radiation at a given time or place, due to advection of H from the surrounding landscape (Glenn et al., 2007). Therefore, it is common for estimated ET to incur 46% (Su, 2002) or greater than 50% error owing to the use of LST in classical sensible heat flux formulation with an aerodynamic resistance (Stewart et al., 1994).

To deal with the problems in the SEB models, Cleugh et al. (2007) developed a remotely sensed ET model using a Penman–Monteith approach driven by MODIS derived vegetation data and daily surface meteorological inputs including incoming solar radiation, surface air temperature and Vapor Pressure Deficit (VPD, the difference between saturated air vapor pressure of a given air temperature and air vapor pressure). Mu et al. (2007a) further modified Cleugh et al.'s model to estimate the global ET (RS-ET). The RS-ET algorithm uses MODIS land cover, albedo, leaf area index (LAI), and Enhanced Vegetation Index (EVI) and a daily meteorological reanalysis data set from NASA's Global Modeling and Assimilation Office (GMAO, v. 4.0.0, 2004) as inputs for regional and global ET mapping and monitoring. Fisher et al. (2008) used Priestley-Taylor method (Priestley and Taylor, 1972) to estimate global ET using AVHRR/NOAA data. Based on Mu et al., 2007a RS-ET model, Zhang et al. (2009) developed a model to estimate ET using remotely sensed Normalized Difference Vegetation Index (NDVI) data; Yuan et al. (2010) modified Mu et al., 2007a RS-ET model by adding the constraint of air temperature to stomatal conductance and calculating the vegetation cover fraction using LAI instead of EVI.

In this paper, we identified problems in the ET algorithm in Mu et al., 2007a paper (hereafter called old algorithm) and solved the problems by improving the old algorithm. In the old algorithm, ET was calculated as the sum of the evaporation from moist soil and the transpiration from the vegetation during daytime. Nighttime ET was assumed to be small and negligible. Soil heat flux (G) was assumed to be zero. For daily calculations, G might be ignored (Gavilána et al., 2007). G is a relatively small component of the surface energy budget relative to sensible and latent energy fluxes for most forest and grassland biomes (Da Rocha et al., 2004; Ogée et al., 2001; Tanaka et al., 2008) and is generally less than 20% of net incoming radiation for the forest and grassland sites from this investigation (e.g. Weber et al., 2007; Granger, http://www.taiga.net/wolfcreek/Proceedings_04.pdf). However, the assumption of negligible G in the old algorithm is a significant concern for tundra. In the Arctic–Boreal regions, G can be a substantial amount of net radiation, especially early in the growing season. The assumption of a negligible G may be valid in mid-latitude regions on a daily basis, however in these areas a substantial portion of net radiation melts ice in the active layer, especially early in the growing season (Engstrom et al., 2006; Harazono et al., 1995). The old algorithm neglected the evaporation from the intercepted precipitation from plant canopy. After the event of precipitation, part of the vegetation and soil surface is covered by water. The evaporation from the saturated soil surface is much higher than the evaporation from the unsaturated soil surface, and the evaporation from the intercepted water by canopy is different from canopy transpiration. In this study, we have improved the old ET algorithm by 1) simplifying the calculation of vegetation cover fraction; 2) calculating ET as the sum of daytime and nighttime components; 3) calculating soil heat flux; 4) improving the methods to estimate stomatal conductance, aerodynamic resistance and boundary layer resistance; 5) separating dry canopy surface from the wet, and hence canopy water loss includes evaporation from the wet canopy surface and transpiration from the dry surface; and 6) dividing soil surface into saturated wet surface and moist surface, and thus soil evaporation includes potential evaporation from the saturated wet surface and actual evaporation from the moist surface. Description of the improvements is detailed in Section 2. We parameterized the improved ET algorithm by using the tower GPP, ET data, the global MODIS GPP and Chen et al.'s global precipitation data (Chen et al., 2002), which is described in Section 5. To examine the performances of the improved ET algorithm, we compared the global ET estimated by the improved ET algorithm with that by the old algorithm and other published studies; we also compared both the old and the improved ET estimates with level 4 ET measured at 46 AmeriFlux sites.

2. Improvements on the MODIS ET algorithm

Terrestrial ET includes evaporation from wet and moist soil, evaporation from rain water intercepted by the canopy before it reaches the ground, the sublimation of water vapor from ice and snow and the transpiration through stomata on plant leaves and stems. Both the old and improved ET algorithms are based on the Penman–Monteith (P–M) equation (Monteith, 1965):

$$\lambda E = \frac{s \times A + \rho \times C_p \times (e_{sat} - e) / r_a}{s + \gamma \times (1 + r_s / r_a)} \quad (1)$$

where λE is the latent heat flux and λ is the latent heat of evaporation; $s = d(e_{sat})/dT$, the slope of the curve relating saturated water vapor pressure (e_{sat}) to temperature; A is available energy partitioned between sensible heat, latent heat and soil heat fluxes on land surface; ρ is air density; C_p is the specific heat capacity of air; and r_a is the aerodynamic resistance. The psychrometric constant γ is given by $\gamma = C_p \times P_a \times M_a / (\lambda \times M_w)$, where M_a and M_w are the molecular masses of dry air and wet air, respectively, and P_a is atmospheric pressure (Maidment, 1993). Surface resistance (r_s) is an effective resistance to evaporation from land surface and transpiration from the plant canopy.

In the old algorithm, ET was calculated as the sum of the evaporation from moist soil and the transpiration from the vegetation during daytime. In the improved algorithm, not only were the

evaporation from the wet soil and the intercepted canopy precipitation included in ET estimates, but also the nighttime ET was calculated as part of the ET. Other improvements of the ET algorithm such as the vegetation cover fraction, the stomatal conductance, the aerodynamic conductance, etc., were made in the improved ET algorithm as follows.

2.1. Vegetation cover fraction

Net radiation is partitioned between the canopy and soil surface based on vegetation cover fraction (F_c). Previously, F_c was calculated as in Eq. (2) (Mu et al., 2007a),

$$Fc = \frac{EVI - EVI_{\min}}{EVI_{\max} - EVI_{\min}} \tag{2}$$

where $EVI_{\min}$ and $EVI_{\max}$ were the minimum and maximum EVI during the study period, set as constants of 0.95 and 0.05 (Mu et al., 2007a), respectively. In the improved algorithm, to reduce numbers of inputs from MODIS datasets and to simplify the procedure and algorithm, we use 8-day 1-km^2 MOD15A2 FPAR (the Fraction of Absorbed Photosynthetically Active Radiation) as a surrogate of vegetation cover fraction (Los et al., 2000) since FPAR and LAI are from a single MODIS product.

$$\mathrm{F_c} = \mathrm{FPAR} \tag{3}$$

2.2. Daytime and nighttime ET

Daily ET should be the sum of daytime and nighttime ET. Previously, the nighttime ET was neglected since most of ET occurs during daytime. In the improved algorithm, we added the nighttime ET. To get nighttime average air temperature (T_{night}), we assume that daily average air temperature (T_{avg}) is the average of daytime air temperature (T_{day}) and T_{night}.

$$T_{night} = 2.0 \times T_{avg} - T_{day} \tag{4}$$

The net incoming solar radiation at night is assumed to be zero. Based on the optimization theory, stomata will close at night to prevent water loss when there is no opportunity for carbon gain (Dawson et al., 2007). In the improved ET algorithm, at night, the stomata are assumed to close completely and the plant transpiration through stomata is zero, except for the transpiration through leaf boundary-layer and leaf cuticles (more details in Section 2.6). Both nighttime and daytime use the same ET algorithm except that different values at daytime and nighttime are used for the same variable.

2.3. Soil heat flux

In both the old and new algorithms, the net incoming radiation to the land surface (R_{net}) is calculated as the Eqs. (12) and (13) in Cleugh et al.'s, 2007 paper.

$$\begin{aligned} R_{net} &= (1-\alpha) \times R_{s\downarrow} + (\varepsilon_a - \varepsilon_s) \times \sigma \times (273.15 + T)^4 \\ \varepsilon_a &= 1 - 0.26 exp^{(-7.77\times10^{-4}\times T^2)} \\ \varepsilon_s &= 0.97 \end{aligned} \tag{5}$$

where α is MODIS albedo, $R_{s\downarrow}$ is the downward shortwave radiation, ε_s is surface emissivity, ε_a is atmospheric emissivity, and T is air temperature in °C.

In the old algorithm, the soil heat flux (G) was directly extracted from the total net incoming radiation (R_{net}) to get the net radiation partitioned in the ET process

$$A = R_{net} - G \tag{6}$$

where (R_{net}) is the net incoming radiation received by land surface and A is the part of (R_{net}) partitioned between latent heat flux and sensible heat flux.

In the improved algorithm, there will be no soil heat flux interaction between the soil and atmosphere if the ground is 100% covered with vegetation. Energy received by soil is the difference between the radiation partitioned on the soil surface and soil heat flux (G).

$$\begin{aligned} A &= R_{net} \\ A_c &= F_c \times A \\ A_{SOIL} &= (1 - F_c) \times A - G \end{aligned} \tag{7}$$

A is available energy partitioned between sensible heat, latent heat and soil heat fluxes on land surface; A_C is the part of A allocated to the canopy and A_{SOIL} is the part of A partitioned on the soil surface. In 1986, Clothier et al. (1986) proposed a method to estimate soil heat flux using remote sensing data as

$$G_{SOIL} = (0.295 - 0.0133 B2/B1) \times A_i \tag{8}$$

where $B1$ and $B2$ are the bandpasses of SPOT filters 610–680 nm, and 790–890 nm, A_i is daytime or nighttime available energy partitioned between latent heat and sensible heat fluxes. Kustas and Daughtry (1990) further improved the method using $B2/B1$ and $NDVI'$.

$$\begin{aligned} G_{SOIL} &= (0.294 - 0.164 B2/B1) \times A_i \\ NDVI' &= (B2 - B1) \Big/ (B1 + B2) \end{aligned} \tag{9}$$

$$G_{SOIL} = (0.325 - 0.208 \times NDVI') \times A_i \tag{10}$$

Daughtry et al. (1990) compared the soil heat flux using different methods with observed data and found that the estimates using $NDVI'$ in Eq. 10 had the lowest absolute error (13%) with a small positive bias. Jacobsen and Hansen (1999) proposed some other methods to estimate G_{SOIL} as,

$$\begin{aligned} G_{SOIL} &= 4.73 \times T_i - 20.87 \\ G_{SOIL} &= (-0.27 \times NDVI + 0.39) \times A_i \end{aligned} \tag{11}$$

$$NDVI = (R_{NIR} - R_{RED}) / (R_{NIR} + R_{RED}) \tag{12}$$

$$G_{SOIL} = (-0.025 \times R_{NIR} / R_{RED} + 0.35) \times A_i \tag{13}$$

where T_i means daytime or nighttime average temperature in °C.

We adopted Eqs. (11) and (12) globally with some constraints. At the extremely hot or cold places or when the difference between daytime and nighttime temperature is low (<5 °C), there is no soil heat flux. The soil heat flux is set to be zero in the old version, now it is estimated as

$$Gsoil = \begin{cases} 4.73 \times T_i - 20.87 & Tmin_{close} \le Tann_{avg} < 25°C,\ Tday - Tnight \ge 5°C \\ 0.0 & Tann_{avg} \ge 25°C \text{ or } Tann_{avg} < Tmin_{close} \text{ or } Tday - Tnight < 5°C \\ 0.39 * A_i & abs(G) > 0.39 \times abs(A_i) \end{cases}$$

$$G = Gsoil \times (1 - F_c) \tag{14}$$

in the improved algorithm, where $Gsoil$ stands for the soil heat flux when $F_C = 0$; $Tann_{avg}$ is annual average daily temperature, and $Tmin_{close}$ is the threshold value below which the stomata will close completely and halt plant transpiration (Mu et al., 2007b; Running et al., 2004).

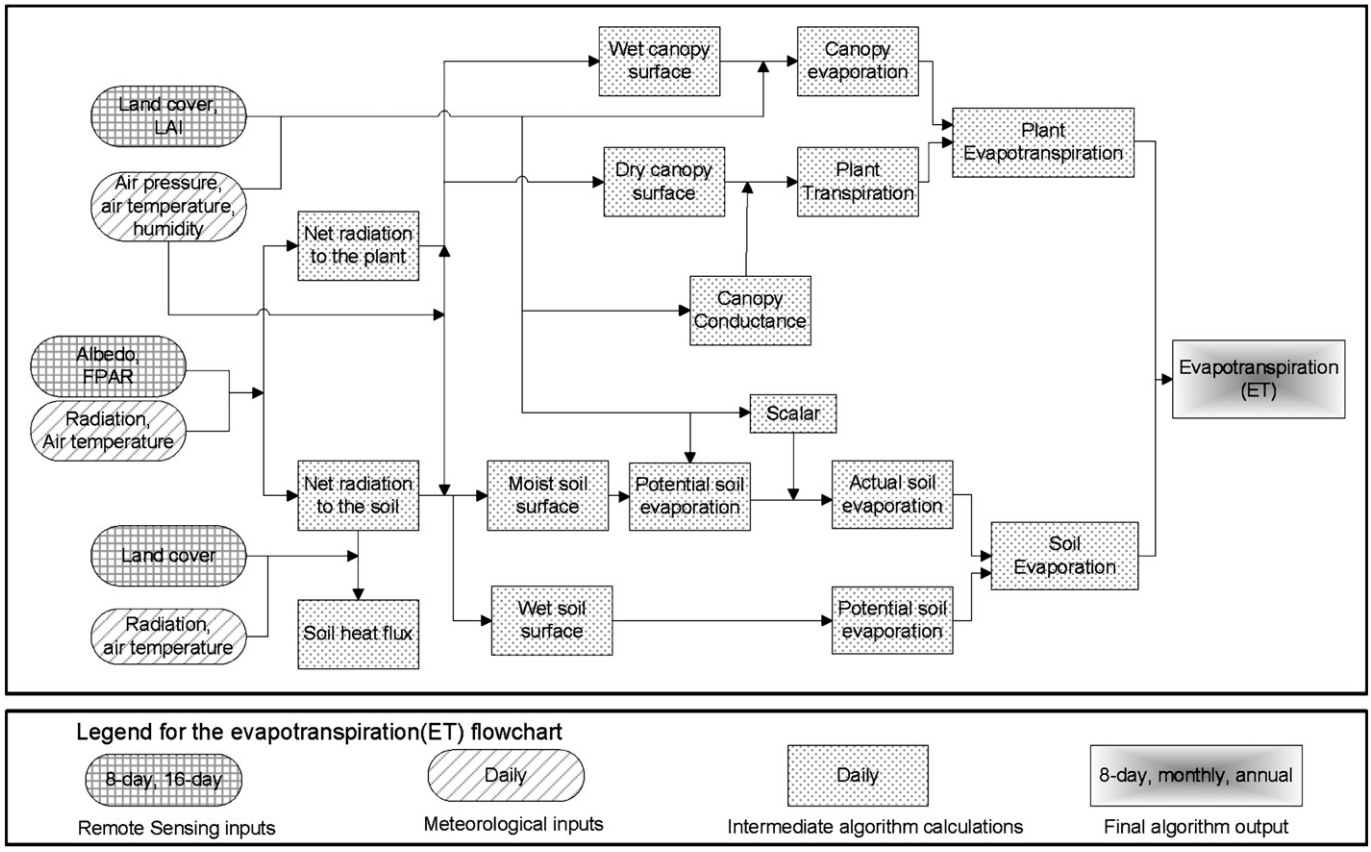

Fig. 1. Flowchart of the improved MODIS Evapotranspiration (ET) algorithm. LAI: leaf area index; FPAR: Fraction of photosynthetically active radiation.

2.4. Wet surface fraction

In the old algorithm, there was no difference between the ET on the saturated and moist bare soil surface, and there was no evaporation but transpiration on the canopy surface (Fig. 1 in Mu et al., 2007a). In the improved ET algorithm, ET is the sum of water lost to the atmosphere from soil surface evaporation, canopy evaporation from the water intercepted by the canopy, and transpiration from plant tissues (Fig. 1). The land surface is covered by the plant and the bare soil surface, and percentage of the two components is determined by F_C. Both the canopy and the soil surface are partly covered by water under certain conditions. The water cover fraction (F_{wet}) is taken from the Fisher et al. (2008) ET model, modified to be constrained to zero when relative humidity (RH) is less than 70%:

$$F_{wet} = \begin{cases} 0.0 & RH < 70\% \\ RH^4 & 70\% \le RH \le 100\% \end{cases} \quad (15)$$

where RH is relative humidity (Fisher et al., 2008). When RH is less than 70%, 0% of the surface is covered by water. For the wet canopy and wet soil surface, the water evaporation is calculated as the potential evaporation as described in Sections 2.5 and 2.7.

2.5. Evaporation from wet canopy surface

Evaporation of precipitation intercepted by the canopy accounts for a substantial amount of upward water flux in ecosystems with high LAI. For the improved algorithm, when the vegetation is covered with water (i.e., F_{wet} is not zero), water evaporation from the wet canopy surface will occur. ET from the vegetation consists of the evaporation from the wet canopy surface and transpiration from plant tissue, whose rates are regulated by aerodynamics resistance and surface resistance.

The aerodynamic resistance ($rhrc$, s m^{-1}) and wet canopy resistance (rvc, s m^{-1}) to evaporated water on the wet canopy surface are calculated as

$$\begin{aligned} rhc &= \frac{1.0}{gl\_sh \times LAI \times Fwet} \\ rrc &= \frac{\rho \times C_p}{4.0 \times \sigma \times T_i^3} \\ rhrc &= \frac{rhc \times rrc}{rhc + rrc} \\ rvc &= \frac{1.0}{gl\_e\_wv \times LAI \times Fwet} \end{aligned} \quad (16)$$

where rhc (s m^{-1}) is the wet canopy resistance to sensible heat, rrc (s m^{-1}) is the resistance to radiative heat transfer through air; gl_sh (s m^{-1}) is leaf conductance to sensible heat per unit LAI, gl_e_wv (m s^{-1}) is leaf conductance to evaporated water vapor per unit LAI, σ (W m^{-2} K^{-4}) is Stefan–Boltzmann constant. Following Biome-BGC model (Thornton, 1998) with revision to account for wet canopy, the evaporation on wet canopy surface is calculated as

$$\lambda E_{wet\_C} = \frac{\left(s \times A_C \times F_C + \rho \times C_p \times (e_{sat} - e) \times F_C / rhrc\right) \times Fwet}{s + \frac{P_a \times C_p \times rvc}{\lambda \times \varepsilon \times rhrc}} \quad (17)$$

where the resistance to latent heat transfer (rvc) is the sum of aerodynamic resistance ($rhrc$) and surface resistance (r_s) in Eq. (1).

Table 1
The Biome Properties Look-Up Table (BPLUT) for MODIS ET. ENF: evergreen needleleaf forest; EBF: evergreen broadleaf forest; DNF: deciduous needleleaf forest; DBF: deciduous broadleaf forest; MF: mixed forest; WL: woody savannas; SV: savannas; CSH: closed shrubland; OSH: open shrubland; Grass: grassland, urban and built-up, barren or sparsely vegetated; Crop: cropland.

Parameter	ENF	EBF	DNF	DBF	MF	CSH	OSH	WL	SV	Grass	Crop
Tmin_open (°C)	8.31	9.09	10.44	9.94	9.50	8.61	8.80	11.39	11.39	12.02	12.02
Tmin_close (°C)	−8.00	−8.00	−8.00	−6.00	−7.00	−8.00	−8.00	−8.00	−8.00	−8.00	−8.00
VPD_close (Pa)	3000	4000	3500	2900	2900	4300	4400	3500	3600	4200	4500
VPD_open (Pa)	650	1000	650	650	650	650	650	650	650	650	650
gl_sh ($m\ s^{-1}$)	0.04	0.01	0.04	0.01	0.04	0.04	0.04	0.08	0.08	0.02	0.02
gl_e_wv ($m\ s^{-1}$)	0.04	0.01	0.04	0.01	0.04	0.04	0.04	0.08	0.08	0.02	0.02
Cl (m/s)	0.0032	0.0025	0.0032	0.0028	0.0025	0.0065	0.0065	0.0065	0.0065	0.0070	0.0070
RBL_MIN ($s\ m^{-1}$)	65.0	70.0	65.0	65.0	65.0	20.0	20.0	25.0	25.0	20.0	20.0
RBL_MAX ($s\ m^{-1}$)	95.0	100.0	95.0	100.0	95.0	55.0	55.0	45.0	45.0	50.0	50.0

2.6. Plant transpiration

2.6.1. Surface conductance to transpiration

Plant transpiration occurs not only during daytime but also at nighttime. Since most of the transpiration occurs at daytime, the nighttime transpiration was neglected in the old algorithm. In the improved algorithm, both the daytime and night time transpiration is included for the calculation of transpiration. For the daytime transpiration, the stomatal conductance estimation has been improved. In the old algorithm, surface conductance (C_C) was estimated by using LAI to scale stomatal conductance (Cs) from leaf level up to canopy level (Landsberg & Gower, 1997),

$$\begin{aligned} C_S &= C_L \times m(Tmin) \times m(VPD) \\ C_C &= C_S \times LAI \end{aligned} \tag{18}$$

where C_L is the mean potential stomatal conductance per unit leaf area, $m(T_{\min})$ is a multiplier that limits potential stomatal conductance by minimum air temperatures ($T_{\min}$), and $m(VPD)$ is a multiplier used to reduce the potential stomatal conductance when VPD (difference between e_{sat} and e) is high enough to reduce canopy conductance (Mu et al., 2007a; Zhao et al., 2005). In the case of plant transpiration, surface conductance is equivalent to the canopy conductance (C_C), and hence surface resistance (r_s) is the inverse of canopy conductance (C_C).

In the old algorithm, C_L was a constant for all biome types. In the improved algorithm, C_L is set differently for different biomes as shown in Table 1 (Kelliher et al., 1995; Schulze et al., 1994; White et al., 2000). In the improved algorithm, the way to calculate C_C has been revised. Canopy conductance to transpired water vapor per unit LAI is derived from stomatal and cuticular conductances in parallel with each other, and both in series with leaf boundary layer conductance (Running & Kimball, 2005; Thornton, 1998).

$$\begin{aligned} r_{corr} &= \frac{1.0}{\frac{101300}{P_a} \times \left(\frac{T_i + 273.15}{293.15}\right)^{1.75}} \\ G_{S\_day}1 &= C_L \times m(Tmin) \times m(VPD) \times r_{corr} \\ G_{S\_night}1 &= 0.0 \\ G_{CU} &= g\_cu \times r_{corr} \\ G_S2 &= gl\_sh \\ C_{C\_i} &= \begin{cases} \frac{G_S2 \times (G_{S\_i}1 + G_{CU})}{G_{S\_i}1 + G_S2 + G_{CU}} \times LAI \times (1.0 - Fwet) & (LAI > 0.0, (1.0 - Fwet) > 0.0) \\ 0.0 & (LAI = 0.0, (1.0 - Fwet) = 0.0) \end{cases} \\ r_{s\_i} &= {}^{1}/_{C_{C\_i}} \end{aligned} \tag{19}$$

where the subscript i means the variable value at daytime and nighttime; $G_{S\_day}1$ and $G_{S\_night}1$ are daytime and nighttime stomatal conductance, respectively; G_{CU} is leaf cuticular conductance; G_S2 is leaf boundary-layer conductance; g_cu is cuticular conductance per unit LAI, set as a constant value of 0.00001 ($m\ s^{-1}$) for all biomes; gl_sh is leaf conductance to sensible heat per unit LAI, which is a constant value for each given biome (Table 1). r_s is the dry canopy surface resistance to transpiration from the plant. Instead of setting the atmospheric pressure (P_a) as a constant value as in the old algorithm, P_a is calculated as a function of the elevation ($Elev$) (Thornton, 1998)

$$\begin{aligned} t_1 &= 1.0 - \frac{LR_{STD} \times Elev}{T_{STD}} \\ t_2 &= \frac{G_{STD}}{LR_{STD} \times \frac{RR}{MA}} \\ P_a &= P_{STD} \times t_1^{t2} \end{aligned} \tag{20}$$

where LR_{STD}, T_{STD}, G_{STD}, RR, MA and P_{STD} are constant values as listed in Table 2. LR_{STD} ($K\ m^{-1}$) is standard temperature lapse rate; T_{STD} (K) is standard temperature at 0.0 m elevation; G_{STD} ($m\ s^{-2}$) is standard gravitational acceleration; RR ($m^3\ Pa\ mol^{-1}\ K^{-1}$) is gas law constant; MA ($kg\ mol^{-1}$) is molecular weight of air and P_{STD} (Pa) is standard pressure at 0.0 m elevation.

Based on the optimization theory, stomata will close at night to prevent water loss when there is no opportunity for carbon gain (Dawson et al., 2007). In the improved ET algorithm, the stomata are assumed to close completely at night, resulting in $G_S1 = 0.0$.

2.6.2. Aerodynamic resistance

The transfer of heat and water vapor from the dry canopy surface into the air above the canopy is determined by the aerodynamic resistance (r_a), which was a constant of 20 $s\ m^{-1}$ in the old algorithm. In the improved algorithm, r_a is calculated as a parallel resistance to convective (rh) and radiative (rr) heat transfer following Biome-BGC model (Thornton, 1998),

$$\begin{aligned} r_a &= \frac{rh \times rr}{rh + rr} \\ rh &= \frac{1.0}{gl\_bl} \\ rr &= \frac{\rho \times C_p}{4.0 \times \sigma \times T_i^3} \end{aligned} \tag{21}$$

where gl_bl ($m\ s^{-1}$) is leaf-scale boundary layer conductance, whose value is equal to leaf conductance to sensible heat per unit

Table 2
Other parameter values as used in the improved ET algorithm.

LR_{STD} ($K\ m^{-1}$)	T_{STD} (K)	G_{STD} ($m\ s^{-2}$)	RR ($m^3\ Pa\ mol^{-1}\ K^{-1}$)	MA ($kg\ mol^{-1}$)	P_{STD} (Pa)
0.0065	288.15	9.80665	8.3143	28.9644e-3	101,325.0

LAI (gl_sh ($m\ s^{-1}$) as in Section 2.5), and σ ($W\ m^{-2}\ K^{-4}$) is Stefan–Boltzmann constant.

2.6.3. Plant transpiration

Finally, the plant transpiration (λE_{trans}) is calculated as

$$\lambda E_{trans} = \frac{\left(s \times A_C \times F_C + \rho \times C_p \times (e_{sat} - e) \times F_C / r_a\right) \times (1 - Fwet)}{s + \gamma \times (1 + r_s / r_a)} \tag{22}$$

where r_a is the aerodynamic resistance calculated from Eq. (21).

In addition, to monitor environmental water stresses and droughts, we also calculate potential surface ET (see Section 2.8). The potential plant transpiration (λE_{POT_trans}) is calculated following the Priestley-Taylor (Priestley and Taylor, 1972).

$$\lambda E_{pot\_trans} = \frac{\alpha \times s \times A_C \times (1 - Fwet)}{s + \gamma}$$
$$\alpha = 1.26 \tag{23}$$

2.7. Evaporation from soil surface

The soil surface is divided into the saturated surface and the moist surface by *Fwet*. The soil evaporation includes the potential evaporation from the saturated soil surface and evaporation from the moist soil surface. The total aerodynamic resistance to vapor transport (r_{tot}) is the sum of surface resistance (r_s) and the aerodynamic resistance for vapor transport (r_v) such that $r_{tot} = r_v + r_s$ (Mu et al., 2007a; van de Griend, 1994). In the old version, a constant r_{totc} ($107\ s\ m^{-1}$) for r_{tot} was assumed globally based on observations of the soil surface in tiger-bush in southwest Niger (Wallace & Holwill, 1997), but it was corrected (r_{corr}) for atmospheric temperature (T_i) and pressure (P_a) (Jones, 1992) with standard conditions assumed to be $T_i = 20$ °C and $P_a = 101300$ Pa.

$$r_{corr} = \frac{1.0}{\frac{101300}{P_a} \times \left(\frac{T_i + 273.15}{293.15}\right)^{1.75}}$$
$$r_{tot} = r_{totc} \times r_{corr}$$
$$r_{totc} = 107.0 \tag{24}$$

We assume that r_v ($s\ m^{-1}$) is equal to the aerodynamic resistance (r_a: $s\ m^{-1}$) in Eq. (1) since the values of r_v and r_a are usually very close (van de Griend, 1994). The aerodynamic resistance at the soil surface (r_{as}) is parallel to both the resistance to convective heat transfer (r_{hs}: $s\ m^{-1}$) and the resistance to radiative heat transfer (r_{rs}: $s\ m^{-1}$) (Choudhury & DiGirolamo, 1998), such that

$$r_{as} = \frac{r_{hs} \times r_{rs}}{r_{hs} + r_{rs}}$$
$$r_{rs} = \frac{\rho \times C_p}{4.0 \times \sigma \times T_i^3}$$
$$r_{hs} = r_{tot} \tag{25}$$

The r_{hs} is assumed to be equal to boundary layer resistance, which is calculated in the same way as total aerodynamic resistance (r_{tot}) in Eq. (24) (Thornton, 1998) except that, in the improved algorithm, r_{totc} is not constant. For a given biome type, there is a maximum (rbl_{max}) and a minimum value (rbl_{min}) for r_{totc}, and r_{totc} is a function of VPD.

$$r_{totc} = \begin{cases} rbl_{max} & VPD \le VPD_{open} \\ rbl_{max} - \frac{(rbl_{max} - rbl_{min}) \times (VPD_{close} - VPD)}{\left(VPD_{close} - VPD_{open}\right)} & VPD_{open} < VPD < VPD_{close} \\ rbl_{min} & VPD \ge VPD_{close} \end{cases} \tag{26}$$

The values of rbl_{max} and rbl_{min}, VPD_{open} (when there is no water stress on transpiration) and VPD_{close} (when water stress causes stomata to close almost completely, halting plant transpiration) are different for different biomes and are listed in Table 1.

The actual soil evaporation (λE_{SOIL}) is calculated in Eq. (27) using potential soil evaporation (λE_{SOIL_POT}) and soil moisture constraint function in the Fisher et al. (2008) ET model. This function is based on the complementary hypothesis (Bouchet, 1963), which defines land–atmosphere interactions from air *VPD* and relative humidity (*RH*, %).

$$\lambda E_{wet\_SOIL} = \frac{\left(s \times A_{SOIL} + \rho \times C_p \times (1.0 - F_C) \times VPD / r_{as}\right) \times Fwet}{s + \gamma \times r_{tot} / r_{as}}$$
$$\lambda E_{SOIL_{POT}} = \frac{\left(s \times A_{SOIL} + \rho \times C_p \times (1.0 - F_C) \times VPD / r_{as}\right) \times (1.0 - Fwet)}{s + \gamma \times r_{tot} / r_{as}}$$
$$\lambda E_{SOIL} = \lambda E_{wet\_SOIL} + \lambda E_{SOIL_{POT}} \times \left(\frac{RH}{100}\right)^{VPD/\beta} \tag{27}$$

where β was set as 100 in the old algorithm, and is revised as 200 in the improved algorithm.

2.8. Total daily evapotranspiration

In the improved algorithm, the total daily ET is the sum of evaporation from the wet canopy surface, the transpiration from the dry canopy surface and the evaporation from the soil surface. The total daily ET and potential ET (λE_{POT}) are calculated in Eq. (28).

$$\lambda E = \lambda E_{wet\_C} + \lambda E_{trans} + \lambda E_{SOIL}$$
$$\lambda E_{POT} = \lambda E_{wet\_C} + \lambda E_{POT\_trans} + \lambda E_{wet\_SOIL} + \lambda E_{SOIL_{POT}} \tag{28}$$

Combination of ET with the potential ET can determine environmental water stress and detect the intensity of drought.

3. Eddy covariance flux towers

The eddy covariance technique is a widely used and accepted method to measure ecosystem-scale mass and energy fluxes. The AmeriFlux network was established in 1996, providing continuous measurements of ecosystem level exchanges of CO_2, water, energy and momentum spanning diurnal, synoptic, seasonal, and interannual time scales and is currently composed of sites from North America, Central America, and South America (http://public.ornl.gov/ameriflux/). AmeriFlux is part of a "network of regional networks" (FLUXNET) including more than 500 tower sites from about 30 regional networks across five continents, providing half-hourly to hourly measurements of carbon dioxide, water vapor, and energy exchanges between terrestrial ecosystems and the atmosphere across a diverse range of ecosystems and climates on a long-term basis (Baldocchi, 2008). The insights and constraints provided by the simultaneous measurement of these fluxes and their corresponding scalar fields ensure that Fluxnet provides an excellent data set for land surface model development and testing.

We obtained the level 4 measured meteorological data and latent heat flux (LE) data at 72 AmeriFlux eddy covariance towers to test the performance of the improved and old algorithms. To ensure a reliable comparison, first, 51 towers were left after we excluded those towers with actual vegetation type different from MOD12 land cover type 2 at any of the surrounding 3×3 1-km2 pixels. Then we further excluded those towers with fewer than half a year of measurements during 2000–2006. As a result, there are 46 AmeriFlux eddy covariance tower sites involved in the evaluation of the algorithms. The tower measured ET in water depth was calculated from tower measured LE data in following equation,

$$ET = \frac{LE}{\lambda} \tag{29}$$

where λ is the latent heat of vaporization (J kg−1). The old and improved ET algorithms were tested at these 46 AmeriFlux eddy covariance tower sites (Table 4, Fig. 2) with available level 4 ET measurements over 2000–2006. These 46 flux towers cover nine typical land cover types and a wide range of climates. The nine land cover types include evergreen needleleaf forest (ENF), evergreen broadleaf forest (EBF), deciduous broadleaf forest (DBF), mixed forest (MF), open shrublands (OSH), close shrublands (CSH), woody savannas (WL), grasslands (Grass), and croplands (Crop).

The AmeriFlux tower data are given every 30 min. When the number (N) of the reliable 30-minute measurements is no less than 40 a day, the daily average values of the incoming solar radiation (*SWrad*), air temperature (*Tavg*), *VPD*, and *LE* are the averages of these measurements. For each 30-minute time period, ET (mm/30 min) is calculated as

$$\begin{aligned} \lambda &= (2.501 - 0.002361 \times T_n) \times 10^6 \\ ET_n &= \frac{LE_n \times 60.0 \times 30.0}{\lambda} \end{aligned} \tag{30}$$

where n is the nth 30-minute observation of each day, λ is calculated using the equation in Maidment's book (Maidment, 1993). When the number of the reliable 30-minute measurements (N) of both LE and T are no less than 40, the daily total ET is calculated as

$$ET = \frac{\sum_{n=1}^{N} ET_n \times 48}{N} \tag{31}$$

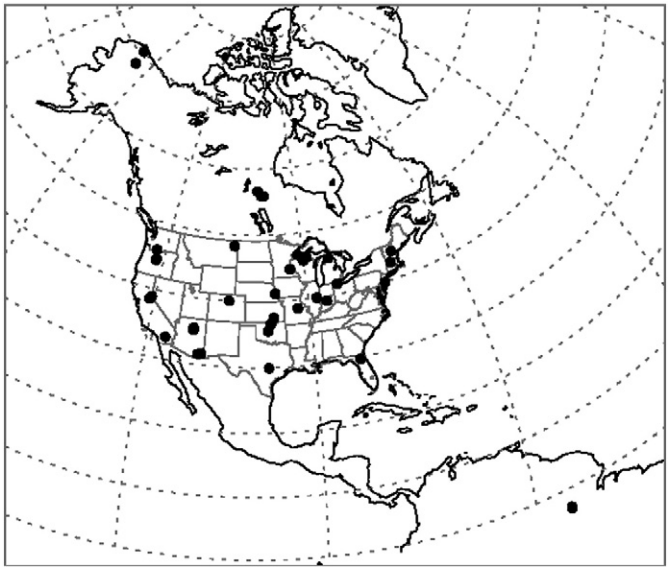

Fig. 2. Distribution of the 46 AmeriFlux eddy flux towers used for validation of the improved ET algorithm.

If N is less than 40, the daily measurements are set as fill value. The daily maximum and minimum air temperature are obtained through the process when calculating the daily average air temperature.

The daytime and nighttime are distinguished by *SWrad*. If *SWrad*>10.0 (W m^{-2}), it's daytime, otherwise, nighttime. The measured daytime *VPD* (*VPDday*) and air temperature (*Tday*), and nighttime VPD (*VPDnight*) and air temperature (*Tnight*) are the averages over daytime and nighttime. When there are fewer than 20 reliable measurements during daytime or nighttime, both daytime and nighttime values are set as fill value.

4. Data and methods

4.1. Input datasets

In Mu et al., 2007a paper, the performance of the old algorithm was tested at 19 AmeriFlux tower sites using two different meteorological datasets in 2001: (1) aggregated daily meteorological data from the half-hour measurements at flux tower sites and (2) the global GMAO meteorological data at 1.00°×1.25° resolution. The input albedo was version 4 0.05-degree CMG albedo. In this study, both old and improved algorithms were driven by the two sets of meteorological data and the ET estimates were compared with the level 4 measured ET at 46 AmeriFlux tower sites.

The input MODIS data to the improved algorithm include 1) global 1-km^2 Collection 4 MODIS land cover type 2 (MOD12Q1) (Friedl et al., 2002); 2) global 1-km^2 MODIS Collection 5 FPAR/LAI (MOD15A2) (Myneni et al., 2002); and 3) Collection 4 0.05-degree CMG MODIS albedo (the 10th band of the White-Sky-Albedo from MOD43C1) (Jin et al., 2003; Salomon et al., 2006; Schaaf et al., 2002). Different from users' expectation, the Collection 5 MODIS FPAR/LAI is being generated with a frozen version of the Colleciton 4 instead of the Colleciton 5 MOD12Q1 land cover as an input by MODIS Adaptive Processing System (MODAPS) at NASA. Due to the limited resources, the climate model grid (CMG, 0.05° resolution) Collection 4 MODIS albedo is used for our MODIS ET because there is no CMG Collection 5 MOD43C1.

4.2. Pre-processing global input data

4.2.1. Spatially interpolating GMAO reanalysis data

The resolution for GMAO (1.00°×1.25°) meteorological data is too coarse for a 1-km^2 MODIS pixel. Zhao et al. (2005) found that, in the Collection 4 MODIS GPP/NPP algorithm (MOD17), each 1-km^2 pixel falling into the same 1.00°×1.25° GMAO grid cell inherited the same meteorological data, creating a noticeable GMAO footprint (Fig. 1a and c in Zhao et al., 2005). Such treatment may be acceptable on a global or regional scale, but it can lead to large inaccuracies at the local scale, especially for terrain with topographical variation or located in regions with steep climatic gradients. To enhance the meteorological inputs, Zhao et al. (2005) have non-linearly interpolated the coarse resolution GMAO data to the 1-km^2 MODIS pixel level based on the four GMAO cells surrounding a given pixel. Theoretically, this GMAO spatial interpolation improves the accuracy of meteorological data for each 1-km^2 pixel because it removes the abrupt changes from one side of a GMAO boundary to the other. In addition, for most World Meteorological Organization (WMO) stations, spatial interpolation reduced the root mean square error (RMSE) and increased the correlation between the GMAO data and the observed WMO daily weather data for 2000–2003, suggesting that the non-linear spatial interpolation considerably improves GMAO inputs. These interpolated GMAO data are, therefore, used in our calculations of ET.

4.2.2. Temporally interpolating MODIS data with bad QC or missing data

The 8-day MOD15A2 LAI/FPAR (Myneni et al., 2002), 16-day MOD43C1 albedo and MODIS EVI (MOD13A2) (Huete et al., 2002)

Table 3
The tower measured annual Gross Primary Production (GPP), tower measured annual Evapotranspiration (ET) summed over all the available days divided by the number of years (≤365 days/year), and Water Use Efficiency (WUE) calculated from Eq. (32) averaged over all the towers for each vegetation type; the annual MODIS GPP averaged over each vegetation type; the expected MODIS ET as calculated from Eq. (33); the actual average annual MODIS ET over each vegetation type. ENF: evergreen needleleaf forest; EBF: evergreen broadleaf forest; DNF: deciduous needleleaf forest; DBF: deciduous broadleaf forest; MF: mixed forest; WL: woody savannas; SV: savannas; CSH: closed shrubland; OSH: open shrubland; Grass: grassland, urban and built-up, barren or sparsely vegetated; Crop: cropland. N/A means that no data is available.

LC	Tower annual GPP ($g\ C\ m^{-2}\ yr^{-1}$)	Tower annual ET ($mm\ yr^{-1}$)	Annual WUE ($g\ C\ mm^{-1}\ m^{-2}$)	Annual MODIS GPP ($g\ C\ yr^{-1}$)	Expected annual MODIS ET ($mm\ yr^{-1}$)	Actual MODIS ET ($mm\ yr^{-1}$)
ENF	978.98	423.64	2.42	876.78	362.89	301.01
EBF	2781.55	1123.03	2.51	2698.53	1073.96	1180.16
DNF	N/A	N/A	N/A	727.00	N/A	334.57
DBF	1303.88	449.44	3.01	1340.12	444.94	533.47
MF	911.17	332.88	2.84	1133.64	398.60	488.12
CSH	909.51	484.82	1.80	811.91	451.88	333.31
OSH	193.60	160.2	1.35	308.79	229.04	272.34
WL	625.81	353.39	1.70	1368.58	805.20	925.62
SV	N/A	N/A	N/A	1209.21	N/A	749.52
Grass	645.68	417.06	1.46	393.09	269.71	352.65
Crop	1089.70	536.79	1.97	883.91	447.82	472.84

contain some cloud-contaminated or missing data (Hill et al., 2006). We temporally filled the missing or unreliable LAI/FPAR, and EVI at each 1-km^2 MODIS pixel based on their corresponding quality assessment data fields as proposed by Zhao et al. (2005). The unreliable CMG MOD43C1 albedo were filled based on the quality control provided with the data. The process entails two steps (see Fig. 5 in Zhao et al., 2005). If the first (or last) 8-day LAI/FPAR (16-day EVI and MOD43C1 albedo) in one year is unreliable or missing, it will be replaced by the closest reliable 8-day (16-day) value. This step ensures that the second step can be performed in which other unreliable LAI/FPAR (EVI, albedo) will be replaced by linear interpolation of the nearest reliable values prior to and after the missing data point.

4.3. Input data for 0.05-degree global MODIS ET data

Since we have the global ET data with the old algorithm at 0.05-degree resolution over 2000–2006, we only compared the performances of the old and new MODIS ET algorithms at 0.05-degree. The input data for the global ET include the 1.00°×1.25° GMAO meteorological data, and the MODIS data as outlined in Section 4.1 over 2000–2006. We used the same method as in Section 4.2.2 to interpolate GMAO data to 0.05° resolution. Both the old and the improved ET algorithms were used to get the global ET estimates at the 0.05° resolution. We filled the unreliable 1-km^2 MODIS input LAI/FPAR and EVI data using the method as mentioned in Section 4.2 (Zhao et al., 2005). The enhanced 1-km^2 MODIS data were aggregated into 25-km^2 by averaging pixels in a 6 by 6 window and further reprojected the Sinusoidal data to 0.05° in geographic projection. The unreliable values in 0.05° MODIS albedo were temporally filled in the same way as in Section 4.2. The 0.05° MODIS land cover type data was generated by choosing the dominant land cover in a 6 by 6 window from the 1-km^2 land cover type.

5. Parameterization of the improved ET algorithm

For parameterization of the improved ET algorithm, we largely follow the method for calibrating parameters of MODIS GPP/NPP algorithm (Zhao et al., 2005). Both MODIS GPP/NPP and MODIS ET algorithms use the same controlling factors from *VPD* and minimum temperature (*Tmin*) on stomatal conductance. We first adopt the parameters of *VPD* and *Tmin* setting from those for MODIS GPP/NPP algorithm (Table 1), then calibrate other parameters for each biome. Below we detail the procedure to parameterize MODIS ET.

The tower derived annual GPP and tower measured annual ET were summed over all the available days divided by the number of years (≤365 days/year). Then the water use efficiency (WUE) for each tower site was calculated as

$$WUE = \frac{GPP}{ET} \tag{32}$$

For a given vegetation type, the tower GPP, ET and WUE are averaged over all the towers with the same biome (Table 3). Finally, the expected annual total ET for a given biome is calculated by using the multiyear mean annual total MODIS GPP (Zhao et al., 2005) and tower-based WUE (listed in Table 3) as

$$ET_{exp} = \frac{MODIS\ GPP}{WUE} \tag{33}$$

We use ET_{exp} as one target (Table 3) to calibrate other parameters in Biome-Property-Look-Up-Table (BPLUT) except *Tmin* and *VPD*, which are directly adopted from MODIS GPP parameters as mentioned above. Each time, the improved ET algorithm is run globally using a set of parameter values at the 0.5° resolution over 2000–2006. The annual MODIS GPP and estimated annual MODIS ET averaged globally for each biome type (ET_{mod}) may greatly differ from the tower GPP and ET_{exp} because, 1) only 46 AmeriFlux tower sites are used to get tower GPP, ET and WUE, and thus they may not represent average conditions for a biome type at the global scale; 2) WUE is the water use efficiency, which should be the ratio of GPP to ET via transpiration. Considering the evaporation included in ET, there is some bias in the calculated WUE and hence ET_{exp} (Law et al., 2002). Therefore, when we calibrate parameters in BPLUT at global scale, not only ET_{mod} is compared to ETexp, but also the spatial pattern of average annual ET over 2000–2006 is compared with Chen et al.'s 0.5° global precipitation data (Chen et al., 2002). At the arid and semi-arid areas, up to 50% or even higher than 100% of the annual precipitation is returned to the atmosphere as ET (Mellouli et al., 2000). At the local scale, the improved ET algorithm is run at the 46 tower sites and the RMSE between the daily ET estimates and ET measurements is calculated. We modify BPLUT and repeat the cycle of comparison till we choose one set of parameter values that perform the best both globally and locally for BPLUT (Table 1). There are no towers with deciduous

Fig. 3. Global annual evapotranspiration with (a) the old version algorithm (b) the improved algorithm and (c) the difference of global annual evapotranspiration (NEW–OLD) between the improved and old versions over 2000–2006. Vegetated regions (using MOD12Q1 land cover type 2) are shown in color, while regions in white are barren or sparsely vegetated areas and non-vegetated areas, including water bodies, snow and ice, and urban areas.

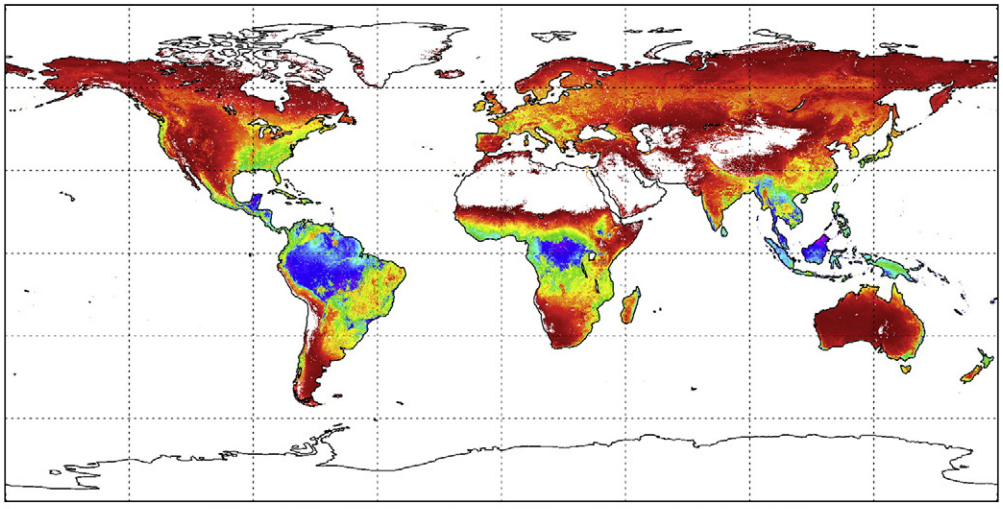


0 250 500 750 1000 1250 1500
Old Annual MODIS ET (2000–2006) mm/yr

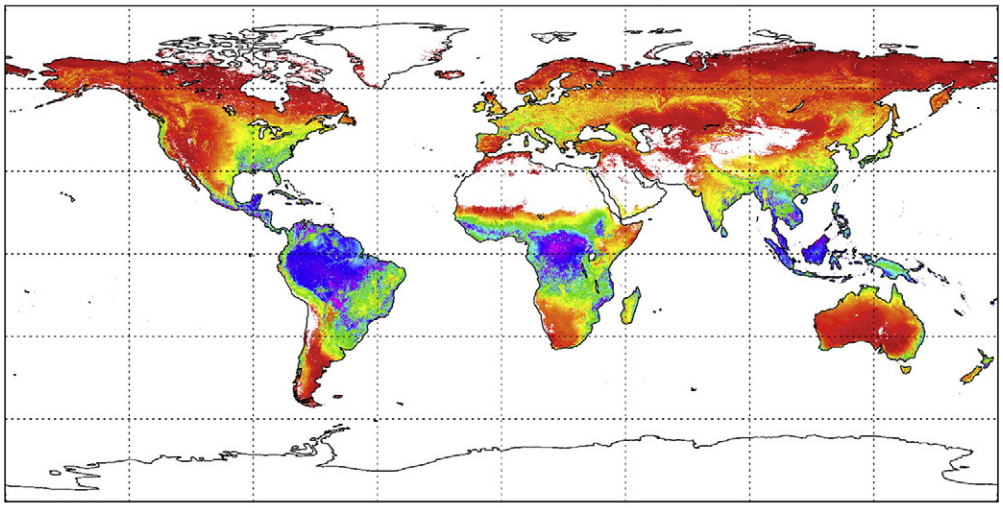


0 250 500 750 1000 1250 1500
New Annual MODIS ET (2000–2006) mm/yr

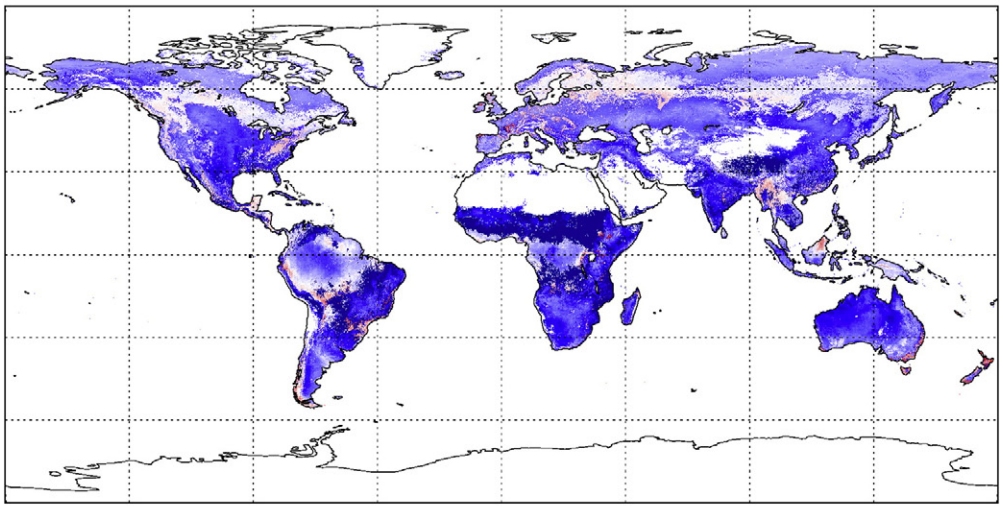


−300 −200 −100 0 100 200 300
ET Difference (NEW−OLD, mm/yr)

needle-leaf forest (DNF) or savannas (SV) in the 46 AmeriFlux towers. We made an assumption that the ET for the DNF should be close to the one for ENF, and the ET for SV should be a little lower than the one for woody savannas.

6. Results and discussion

6.1. Implementing ET algorithm at the global scale

The old and improved ET algorithms were implemented globally over 2000–2006 at a resolution of 0.05° using the preprocessed MODIS remote sensing data and the GMAO meteorological data as detailed in Section 4.2. Fig. 3a and b show that both algorithms have the highest ET over the tropical forests, whereas dry areas and areas with short growing seasons have the lowest estimates of ET. The ET for temperate and boreal forests lies between the two extremes (Fig. 3a and b). The difference in the global annual ET between the improved and old algorithms in Fig. 3c shows that the improved algorithm generally enhances the global annual ET, especially at the semi- and arid regions, with an average of 568 ± 378 mm year^{-1} over vegetated land areas (Fig. 4). The global ET with the old algorithm has a global average of 416 mm year$^{-1} \pm 337$ mm year^{-1}. The histograms of the global annual ET by both algorithms in Fig. 4 also demonstrate that the old algorithm underestimated ET in the semi- and arid areas while overestimates ET in areas with the highest ET, such as part of the Amazon, Africa and tropic rainforests (Figs. 3c and 4). The improved ET algorithm lowers the ET estimates over some areas of high latitudes in the northern hemisphere (Fig. 3c).

Based on MOD12Q1 land cover types 2, barren/deserts take up 24% of the Earth's land surface. If we assume that the ET from the barren/deserts is zero, the average MODIS ET estimate with the improved algorithm over the entire land surface is $568*(100-24)/100 = 431.68$ mm year^{-1}. In reality, ET at the barren/deserts is not zero, so the ET estimates should be in the range of a little higher than 431.68 mm year^{-1}. Over the entire land surface of the globe, precipitation averages around 750 mm year^{-1} (Fisher et al., 2005). Some studies concluded that ET returns more than 60% of precipitation on land back to the atmosphere (Korzoun et al., 1978; L'vovich & White, 1990). Based on these published data, the actual ET over the global land surface should be around $750*60\% = 450$ mm year^{-1}. Our average MODIS ET estimate by the improved algorithm over the complete land surface is very close to the actual ET calculated from precipitation. The MODIS ET estimate with the old algorithm over the vegetated area (416 mm year^{-1}) was less than the actual ET (450 mm year^{-1}) over the entire land surface.

Averaged over 2000–2006, the total global annual ET over the vegetated land surface with the improved algorithm is 62.8×10^3 km^3, much higher than 45.8×10^3 km^3 with the old algorithm, and a little less than 65.5×10^3 km^3 reported by Oki and Kanae (2006), because our MODIS ET doesn't include urban and barren areas since there is no MODIS derived FPAR/LAI for these land cover types.

Fig. 5 shows zonal mean of global annual ET by both algorithms. The old algorithm overestimated ET at very high latitudes where the growing season is so short that the actual ET should be much less than 1000 mm year^{-1} (Fig. 5). Liski et al. (2003) reported that the ET in boreal and temperate forests across Europe (34 sites) ranged from 328 to 654 mm year^{-1}, while the average ET was 466 mm yr^{-1} for Canada (18 sites) and 642 mm year^{-1} for the US and Central America (26 sites) for biomes ranging from arctic tundra to tropical rainforest. The improved ET estimates are within the range of these reported ET from field data.

6.2. Algorithm performance at the eddy flux tower sites

As shown in Table 4, within the nine land cover types among the towers, the improved ET algorithm enhances the ET estimates the most at woody savannas, grasslands and croplands, while the improved ET estimates have no big differences from the ET estimates by the old algorithm over the forests. For each of the seven biome types among the 46 flux towers except for CSH and OSH since there is only one tower with fewer than 365 measurements for each of them, we chose one tower to show the performance of the improved algorithm against the old algorithm (Fig. 6). The left panel (Fig. 6a, c, e, g, i, k and m) shows the comparison of the ET measurements to the ET estimates with the old algorithm, while the right panel (Fig. 6b, d, f, h, j, l and n) shows the comparison to the ET estimates with the improved algorithm. Over the grasslands, croplands and woody savanna, the old algorithm underestimated the ET. The improved algorithm enhances the ET estimates significantly. For the towers Tonzi Ranch (WL), Walnut River (Grass), Bondville (Crop), the improved ET estimates capture the magnitude of the daily ET observations better than the old algorithm. For example, at Tonzi Ranch, the improved algorithm reduced the RMSE of the daily ET estimates from 0.75 mm day^{-1} to 0.67 mm day^{-1} driven by tower meteorological data, and from 0.79 mm day^{-1} to 0.68 mm day^{-1} driven by the GMAO meteorological data (Table 4). For the forest towers such as Donaldson (ENF), Amazonian Tapajos KM67 Mature Forest (EBF), Willow Creek (DBF) and Little Prospect Hill (MF), although the daily RMSE of the improved ET are higher than that of the old ET, daily average improved ET estimates have smaller MAEs than the old ET (Table 4). For instance, at Donaldson, the improved algorithm has higher RMSE (1.30 and 1.49 mm day^{-1}) than the old algorithm (1.06 and 1.10 mm day^{-1}) driven by tower and GMAO meteorological data, respectively; however, the magnitude of the improved daily ET is much closer to the tower-measured ET (Fig. 6a and b) and the improved algorithm has lower MAE (0.29 and 0.45 mm day^{-1}) than the old algorithm (0.70 and 0.62 mm day^{-1}) driven by tower and GMAO meteorological data, respectively. We use the Taylor skill score (Taylor, 2001) to evaluate the skill of the performances (Table 4).

$$S = \frac{4 \times (1 + R)}{(\hat{\sigma} + 1/\hat{\sigma})^2 \times (1 + R_0)} \tag{34}$$

where R is the correlation coefficient, R_0 is theoretical maximum correlation, and $\hat{\sigma}$ is the standard deviation of ET estimates normalized by the standard deviation of ET measurements. The improved algorithm has higher scores at Donaldson (Table 4) which

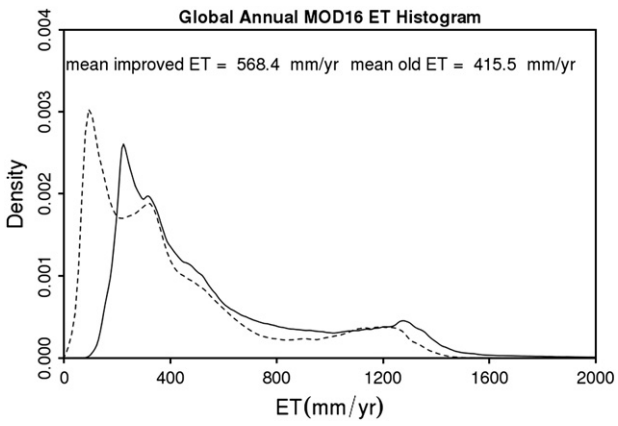

Fig. 4. Comparison of the histograms of climatological average of global annual evapotranspiration with the old version algorithm (dashed line) and with the improved algorithm (solid line) over 2000–2006. The global average ET with the old version is 415.5 mm/year and 568.4 mm/year with the improved algorithm (see text). These comparisons are only for vegetated land surfaces. The vegetated land area is shown as the colored area in Fig. 3.

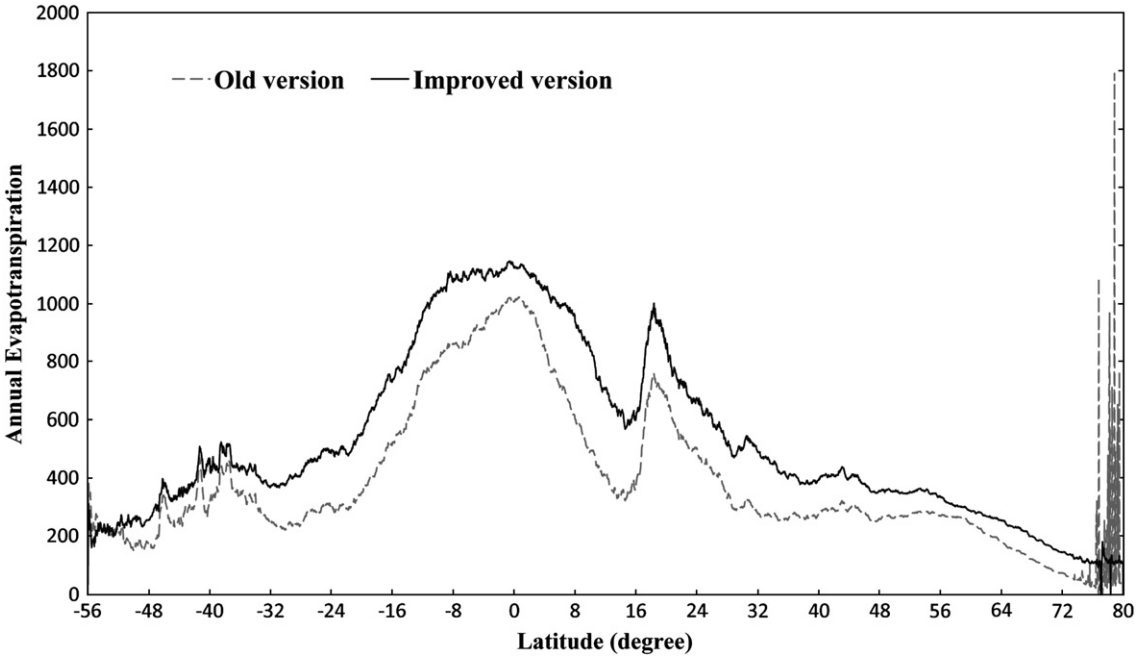

Fig. 5. Comparison of the climatological zonal mean of global annual evapotranspiration with the old version algorithm (grey dashed line) and with the improved algorithm (solid black line) over 2000–2006. Overestimated ET at the high latitude in the north hemisphere with old version are lowered down with the improved algorithm. These comparisons are only for vegetated land surfaces. The vegetated land area is shown as the colored area in Fig. 3.

implies that the improved algorithm performances better at Donaldson than the old one.

Relative to the old algorithm, the improved algorithm reduces average daily ET MAE across the 46 towers from 0.39 mm day^{-1} to 0.33 mm day^{-1} (tower-specific meteorology) and from 0.40 mm day^{-1} to 0.31 mm day^{-1} (GMAO meteorology), indicating that the improved ET estimates capture the magnitudes of the ET measurements better than the old algorithm. The improved MAE values are 24.6% (tower-specificmeteorology) and 24.1% (GMAO meteorology) of the ET measurements by the improved algorithm, within the 10–30% range of the accuracy of ET observations (Courault et al., 2005; Jiang et al., 2004; Kalma et al., 2008). At the 46 tower sites, the MAE from the improved ET algorithm is significantly better than the MAE from the old ET algorithm, with one-tailed $p<0.06$ driven by tower meteorological data and $p<0.01$ driven by GMAO data. The improved algorithm slightly increases the average RMSE of daily ET (Fig. 7; Table 4) from 0.81 mm day^{-1} to 0.84 mm day^{-1} and from 0.88 mm day^{-1} to 0.90 mm day^{-1} (GMAO meteorology), and decreases the average correlation coefficients between the daily ET estimates and measurements from 0.64 to 0.58 (GMAO meteorology) and from 0.71 to 0.65 (tower-specific meteorology) (Table 4). However, the new scores of 0.55 (tower-specific) and 0.53 (GMAO) across the 46 towers are higher than 0.50 and 0.46 with the old algorithm (Table 4), indicating that overall, the improved algorithm performances better at the 46 towers.

Fig. 7 shows the comparisons of the average ET observations to the average daily ET estimates with the old and the improved algorithms across all the available days at the 46 flux tower sites. Both algorithms were driven by tower-specific meteorology (Fig. 7a and c) and the global GMAO meteorology (Fig. 7b and d). The improved ET algorithm increases the correlation coefficients of the ET observations with tower-driven ET estimates from 0.83 (Fig. 7a) to 0.86 (Fig. 7c), and from 0.81 (Fig. 7b) to 0.86 (Fig. 7d) driven by GMAO meteorology.

6.3. Discussion

The existing biases between the ET estimates and the ET measurements arises from below major causes,

1) Algorithm input data. Uncertainties from MODIS LAI/FPAR (Demarty et al., 2007; Yang et al., 2006) and daily GMAO meteorological data (Zhao et al., 2006) can introduce biases to ET estimates. Heinsch et al. (2006) compared tower meteorological data with GMAO data, and the 1-km^2 Collection 4 MODIS LAI (MOD15) and MODIS land cover (MOD12) with ground-based measurements, finding existing biases in both the GMAO data and the MODIS data when compared to observations. The biases in GMAO meteorological data while approximately 62% of MODIS LAI estimates were within the estimates based on field optical measurements, remaining values overestimated site values (Heinsch et al., 2006). Comparison of LAI at the patch level can significantly improve the agreements, but the Collection 3 MODIS LAI still tends to be higher (Wang et al., 2004). Overestimates of LAI may result in overestimates of ET even if other input data such as the meteorological data and MODIS albedo data are relatively accurate. Although the temporal filling of unreliable MODIS data, including LAI, FPAR and albedo, greatly improves the accuracy of inputs, the filled values are artificial and contain uncertainties. There is a hypothesis that all the uncertainties associated with the MODIS data are contained in the quality flags MODIS QA, an assumption which proved efficient for reducing the weight of unreliable satellite products, especially over tropical forests (Demarty et al., 2007). However, the MODIS QA remains a qualitative measure of uncertainty, and does not quantitatively accounts for each source of error in the MODIS data retrieval procedure (sensor calibration, atmospheric corrections, land cover mapping radiative transfer forward and inverse modelling) (Demarty et al., 2007). Also, the inaccuracy in MODIS FPAR will lead to miscalculation of Fc, and hence ET. All of these uncertainties from inputs can introduce biases in ET estimates that are difficult to detect.
2) Inaccuracy in the measured data. Currently, the ground data from the eddy covariance flux towers provide the best ET estimates. However, they have an error or uncertainties of about 10–30% based on comparison of multiple towers at the same site, or by comparison with independent measurements of ET by other methods such as lysimeters or sap flux sensors (Glenn, Morino,

Table 4
The tower names, abbreviations, latitude (lat), longitude (lon), biome types in the parentheses, number of days with valid tower measurements (Days), average daily tower evapotranspiration measurements over all the days with valid values (ET_OBS: mm/day), daily root mean square error (RMSE: mm/day), mean absolute bias (MAE: mm/day), the contribution of night time ET to daily total ET driven by GMAO meteorological data (%, Night), the ratio of soil heat flux to daily LE (%, G) driven by GMAO meteorology, correlation coefficient (R) and Taylor skill score (S) of Evapotranspiration for the 46 AmeriFlux eddy flux towers. 1: tower-driven results from the old version; 2: GMAO-driven results from the old version; 3: tower-driven results from the improved version; 4: GMAO-driven results from the improved version.

Site	Abbrev.	lat	lon	Days	ET_OBS	RMSE1	RMSE2	RMSE3	RMSE4	Night	G	MAE1	MAE2	MAE3	MAE4	R1	R2	R3	R4	S1	S2	S3	S4	Citations
ARM_SGP_Main	USARM (Crop)	36.6	−97.5	1129	1.43	1.03	1.00	1.06	1.00	21.39	2.18	0.74	0.67	0.62	0.3	0.6	0.57	0.42	0.41	0.27	0.21	0.76	0.71	
Bondville	USBo1 (Crop)	40.0	−88.3	1616	1.82	1.13	1.13	0.96	1.03	8.46	1.08	0.76	0.67	0.3	0.16	0.76	0.74	0.78	0.73	0.19	0.16	0.54	0.61	
Mead_Irrigated	USNe1 (Crop)	41.2	−96.5	1080	1.62	1.42	1.43	1.16	1.18	10.02	1.85	0.91	0.84	0.6	0.48	0.89	0.84	0.87	0.81	0.14	0.14	0.45	0.70	
Mead_Irrigated_Rotation	USNe2 (Crop)	41.2	−96.5	1022	1.56	1.41	1.41	1.17	1.18	10.66	1.61	0.9	0.84	0.62	0.48	0.87	0.84	0.85	0.8	0.02	0.01	0.12	0.05	
Mead_Rainfed	USNe3 (Crop)	41.2	−96.4	1027	1.46	1.19	1.18	0.95	0.97	10.40	1.78	0.8	0.73	0.47	0.35	0.89	0.85	0.85	0.79	0.05	0.05	0.31	0.45	
Rosemount_G19_Alternative_ Management_Corn_ Soybean_Rotation	USRo3 (Crop)	44.7	−93.1	573	1.35	0.97	0.96	0.82	0.79	7.35	1.51	0.6	0.61	0.22	0.21	0.77	0.76	0.72	0.75	0.39	0.41	0.38	0.50	
Rosemount_G21_Conventional_ Management_Corn_ Soybean_Rotation	USRo1 (Crop)	44.7	−93.1	574	1.39	1.04	1.04	0.85	0.82	7.42	1.52	0.66	0.66	0.27	0.26	0.72	0.71	0.71	0.72	0.32	0.23	0.32	0.23	
Sky_Oaks_Old	USSO2 (CSH)	33.4	−116.6	333	1.04	0.89	1.00	1.10	0.93	67.01	5.26	0.54	0.67	0.71	0.51	0.21	−0.02	0.02	0.06	0.80	0.86	0.86	0.82	
Bartlett_Experimental_Forest	USBar (DBF)	44.1	−71.3	614	0.84	0.97	1.18	0.95	1.03	−0.85	1.18	0.55	0.77	0.48	0.66	0.9	0.81	0.9	0.83	0.54	0.46	0.68	0.58	Jenkins et al., 2007
Missouri_Ozark	USMOz (DBF)	38.7	−92.2	606	2.20	0.92	1.07	0.95	1.04	0.95	1.71	0.1	0.07	0.03	0.08	0.83	0.74	0.84	0.76	0.25	0.25	0.10	0.16	
Morgan_Monroe_State_Forest	USMMS (DBF)	39.3	−86.4	1483	1.16	0.67	0.87	0.71	0.81	−2.57	1.60	0.27	0.39	0.27	0.27	0.88	0.81	0.88	0.82	0.20	0.24	0.43	0.53	
Ohio_Oak_Openings	USOho (DBF)	41.6	−83.8	371	1.94	0.78	0.84	0.79	0.83	−0.60	0.85	0.07	0.02	0.14	0.17	0.85	0.83	0.86	0.83	0.88	0.88	0.44	0.29	
UMBS	USUMB (DBF)	45.6	−84.7	1205	1.22	0.45	0.64	0.48	0.60	−1.58	0.69	0.01	0.11	0.02	0.05	0.94	0.88	0.93	0.89	0.06	0.08	0.25	0.36	
Willow_Creek	USWCr (DBF)	45.8	−90.1	1246	0.97	0.56	0.84	0.59	0.76	−1.75	1.28	0.25	0.39	0.18	0.35	0.91	0.83	0.91	0.85	0.37	0.27	0.77	0.89	Cook et al., 2004
LBA_Tapajos_KM67_ Mature_Forest	BRSa1 (EBF)	−2.9	−55.0	1008	3.08	0.67	1.18	0.72	1.28	3.83	0.00	0.35	0.28	0.44	0.11	0.74	0.34	0.76	0.33	0.27	0.14	0.64	0.17	Hutyra et al., 2007; Rocha et al., 2009; Fisher et al., 2009
LBA_Tapajos_KM83_ Logged_Forest	BRSa3 (EBF)	−3.0	−55.0	1281	3.63	1.05	1.39	0.91	1.39	4.65	0.00	0.7	0.62	0.29	0.45	0.61	0.37	0.62	0.35	0.04	0.07	0.65	0.73	
Blodgett_Forest	USBlo (ENF)	38.9	−120.6	1586	1.99	1.11	1.48	1.11	1.41	3.81	2.21	0.57	0.66	0.57	0.58	0.65	0.19	0.65	0.24	0.84	0.49	0.87	0.35	
Donaldson	USSP3 (ENF)	29.8	−82.2	1585	2.68	1.06	1.10	1.30	1.49	16.86	1.29	0.57	0.5	0.28	0.51	0.65	0.56	0.52	0.48	0.57	0.56	0.80	0.50	Gholz & Clark, 2002; Clark et al., 2004
Flagstaff_Unmanaged_Forest	USFuf (ENF)	35.1	−111.8	308	1.24	0.81	0.99	0.92	1.00	3.40	−0.32	0.44	0.51	0.59	0.61	0.62	0.33	0.62	0.42	0.93	0.92	0.66	0.72	
Metolius_First_Young_Pine	USMe5 (ENF)	44.4	−121.6	545	0.99	0.60	0.57	0.60	0.58	−0.70	1.60	0.06	0.06	0.11	0.01	0.28	0.29	0.25	0.26	0.11	0.10	0.28	0.26	Anthoni et al., 2002
Metolius_Intermediate_Pine	USMe2 (ENF)	44.5	−121.6	707	1.18	0.76	0.76	0.77	0.79	−0.19	2.28	0.08	0.07	0.08	0.1	0.34	0.31	0.32	0.29	0.10	0.09	0.25	0.24	Thomas et al., 2009

Metolius_New_Young_Pine	USMe3 (ENF)	44.3	−121.6	361	0.93	0.61	0.54	0.66	0.57	−3.58	2.63	0.28	0	0.37	0.12	0.4	0.42	0.39	0.38	0.19	0.18	0.41	0.40	Vickers et al., 2010
Niwot_Ridge	USNR1 (ENF)	40.0	−105.5	1535	1.54	0.97	1.01	0.96	1.00	−1.26	7.83	0.67	0.65	0.66	0.69	0.68	0.6	0.68	0.64	0.64	0.61	0.60	0.59	
UCI_1850	CANS1 (ENF)	55.9	−98.5	429	0.56	0.38	0.41	0.51	0.51	−0.63	−1.03	0.1	0.08	0.1	0.04	0.82	0.78	0.74	0.7	0.55	0.44	0.56	0.52	
UCI_1930	CANS2 (ENF)	55.9	−98.5	431	0.57	0.32	0.38	0.41	0.43	−0.69	−0.78	0.09	0.09	0.08	0.03	0.86	0.8	0.78	0.75	0.24	0.27	0.14	0.26	
UCI_1964	CANS3 (ENF)	55.9	−98.4	488	0.54	0.35	0.40	0.50	0.51	2.09	−0.77	0.04	0.08	0.12	0.11	0.83	0.79	0.75	0.73	0.85	0.85	0.77	0.85	
UCI_1964wet	CANS4 (ENF)	55.9	−98.4	236	0.38	0.40	0.50	0.50	0.58	0.39	−1.37	0.18	0.28	0.24	0.27	0.76	0.82	0.71	0.76	0.91	0.87	0.85	0.87	
UCI_1981	CANS5 (ENF)	55.9	−98.5	503	0.58	0.38	0.50	0.58	0.65	3.17	−0.50	0.07	0.14	0.18	0.19	0.84	0.77	0.77	0.71	0.65	0.57	0.46	0.48	
UCI_1989	CANS6 (ENF)	55.9	−99.0	494	0.53	0.35	0.39	0.48	0.48	1.25	−1.01	0.06	0.06	0.14	0.09	0.84	0.79	0.76	0.72	0.92	0.91	0.92	0.92	
UCI_1998	CANS7 (ENF)	56.6	−99.9	411	0.59	0.33	0.37	0.39	0.44	−8.98	−0.52	0.11	0.11	0.11	0.17	0.84	0.77	0.74	0.69	0.34	0.39	0.67	0.72	
Wind_River_Crane_Site	USWrc (ENF)	45.8	−122.0	974	1.54	1.08	0.96	1.71	1.28	7.84	0.62	0.31	0.21	0.94	0.67	0.48	0.41	0.48	0.41	0.32	0.36	0.67	0.70	
Wisconsin_Mature_Red_Pine	USWi4 (ENF)	46.7	−91.2	308	2.09	1.16	1.24	1.60	1.70	13.33	1.27	0.25	0.14	0.34	0.41	0.39	0.28	0.29	0.25	0.07	0.03	0.30	0.15	
ARM_SGP_Burn	USARb (Grass)	35.5	−98.0	553	2.15	1.30	1.35	0.85	0.88	12.85	0.83	0.98	0.96	0.51	0.43	0.89	0.84	0.9	0.86	0.76	0.75	0.46	0.43	
ARM_SGP_Control	USARc (Grass)	35.5	−98.0	554	2.36	1.54	1.56	1.10	1.04	12.61	0.82	1.21	1.16	0.77	0.63	0.9	0.84	0.9	0.86	0.32	0.22	0.89	0.78	
Atqasuk	USAtq (Grass)	70.5	−157.4	244	0.11	0.45	0.45	0.50	0.53	7.36	0.00	0	0.02	0.02	0.16	0.25	0.23	0.11	−0.03	0.85	0.84	0.63	0.70	
Audubon_Grasslands	USAud (Grass)	31.6	−110.5	1431	0.78	0.81	0.81	0.81	0.79	52.58	2.35	0.48	0.45	0.37	0.07	0.69	0.63	0.47	0.4	0.86	0.82	0.73	0.74	
Kendall_Grassland	USWkg (Grass)	31.7	−109.9	929	0.63	0.65	0.64	0.68	0.70	23.92	2.10	0.45	0.39	0.19	0	0.5	0.52	0.27	0.26	0.85	0.80	0.62	0.62	
Walnut_River	USWlr (Grass)	37.5	−96.9	885	1.86	1.00	1.05	0.68	0.75	45.37	1.77	0.36	0.33	0.3	0.11	0.68	0.63	0.51	0.46	0.34	0.19	0.22	0.13	
Fort_Peck	USFPe (Grass)	48.3	−105.1	1095	0.77	0.81	0.77	0.80	0.81	10.37	0.67	0.78	0.77	0.15	0.2	0.87	0.84	0.85	0.8	0.91	0.80	0.62	0.56	
Fort_Dix	USDix (MF)	40.0	−74.4	412	1.56	0.74	0.79	1.25	1.63	15.63	0.25	0.01	0.28	0.43	0.87	0.75	0.77	0.69	0.68	0.69	0.65	0.51	0.54	
Little_Prospect_Hill	USLPH (MF)	42.5	−72.2	667	1.35	0.61	0.87	1.25	1.37	15.67	0.50	0.18	0.43	0.81	0.83	0.9	0.84	0.86	0.76	0.73	0.71	0.66	0.54	Hadley et al., 2008
Sylvania_Wilderness	USSyv (MF)	46.2	−89.3	825	0.89	0.59	0.76	1.00	1.13	9.42	0.25	0.26	0.38	0.47	0.62	0.9	0.83	0.81	0.78	0.95	0.90	0.93	0.92	Desai et al., 2005
Ivotuk	USIvo (OSH)	68.5	−155.8	210	0.19	0.23	0.26	0.31	0.34	6.00	0.00	0.03	0.1	0.02	0.02	0.64	0.53	0.35	−0.01	0.59	0.42	0.92	0.86	
Flagstaff_Wildfire	USFwf (WL)	35.4	−111.8	338	0.94	0.68	0.69	0.84	0.75	47.89	−0.49	0.45	0.42	0.43	0.31	0.65	0.57	0.24	0.35	0.94	0.82	0.86	0.87	
Freeman_Ranch_Mesquite_Juniper	USFR2 (WL)	29.9	−98.0	649	2.08	1.08	0.95	0.91	0.85	14.13	0.68	0.65	0.54	0.1	0.29	0.72	0.81	0.69	0.79	0.33	0.51	0.10	0.31	
Tonzi_Ranch	USTon (WL)	38.4	−121.0	1342	1.13	0.75	0.79	0.67	0.68	20.42	4.59	0.2	0.19	0.01	0.02	0.73	0.68	0.78	0.75	0.70	0.64	0.37	0.32	Baldocchi et al., 2004; Xu & Baldocchi, 2003
Average					1.34	0.81	0.88	0.84	0.90	9.53	1.09	0.39	0.40	0.33	0.31	0.71	0.64	0.65	0.58	0.50	0.46	0.55	0.53	

et al., 2008b). Also, the eddy covariance flux towers have an energy balance closure problem that, the sum of the net radiation and the ground heat flux, was found in most cases to be larger than the sum of turbulent fluxes of latent heat and sensible heat (Aubinet, 2000; Wilson et al., 2002). Correcting error and reducing uncertainty in the ET measurements are still uncertain due to the closure error (Shuttleworth, 2007). Scott (2010) used the watershed water balance to evaluate the accuracy of eddy

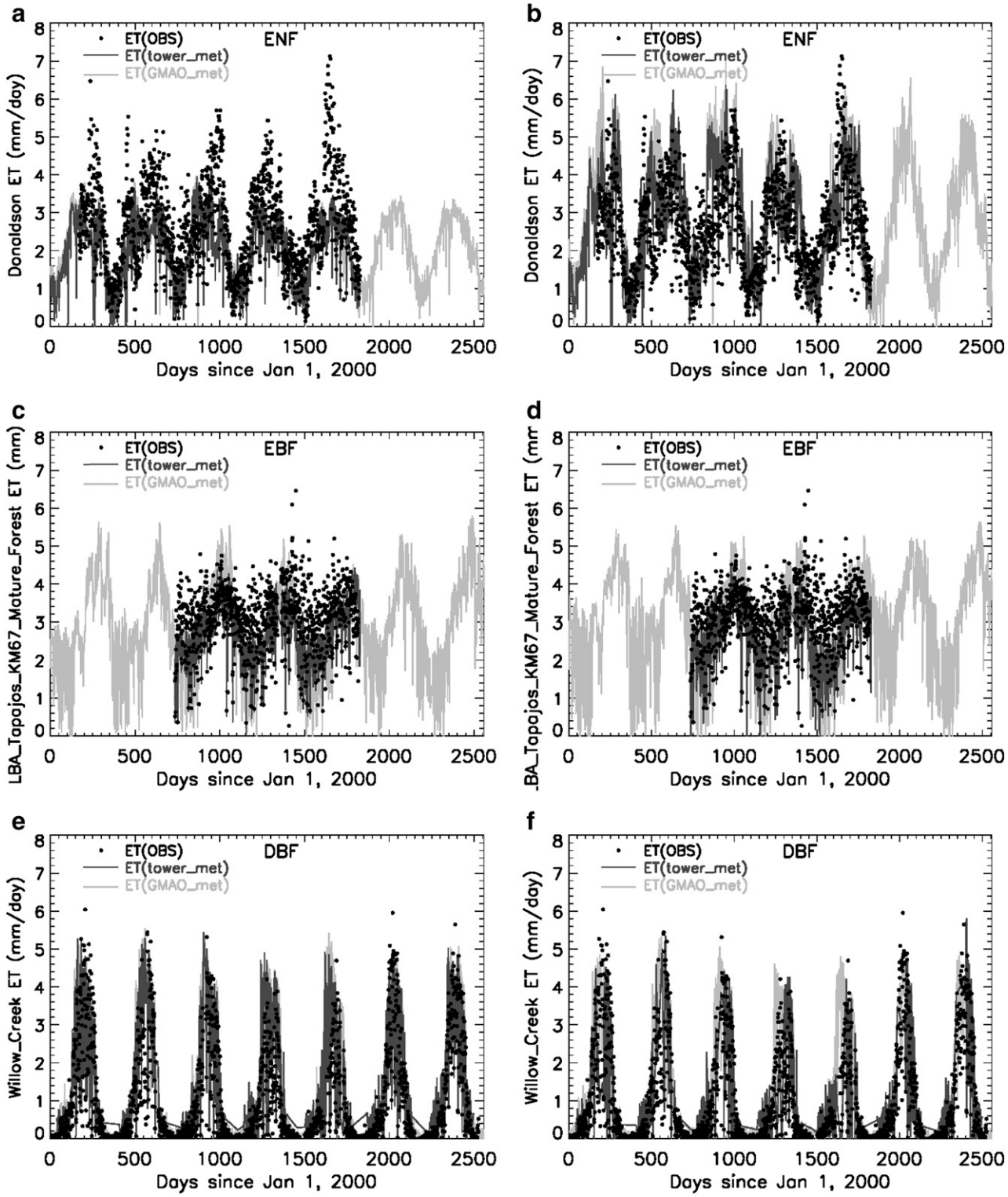

Fig. 6. The ET measurements (black dots, OBS), the ET estimates with the old version (the left panel, a, c, e, g, i, k, and m) and the improved MODIS ET algorithm (the right panel, b, d, f, h, j, l, and n) driven by flux tower measured meteorological data (tower_met, black lines) and GMAO meteorological data (GMAO_met, grey lines) over 2000–2006 at seven tower sites, Donaldson (a and d), LBA Tapajos KM67 Mature Forest (c and d), Willow Creek (e and f), Little Prospect Hill (g and h), Tonzi Ranch (i and j), Walnut River (k and l) and Bondville (m and n).

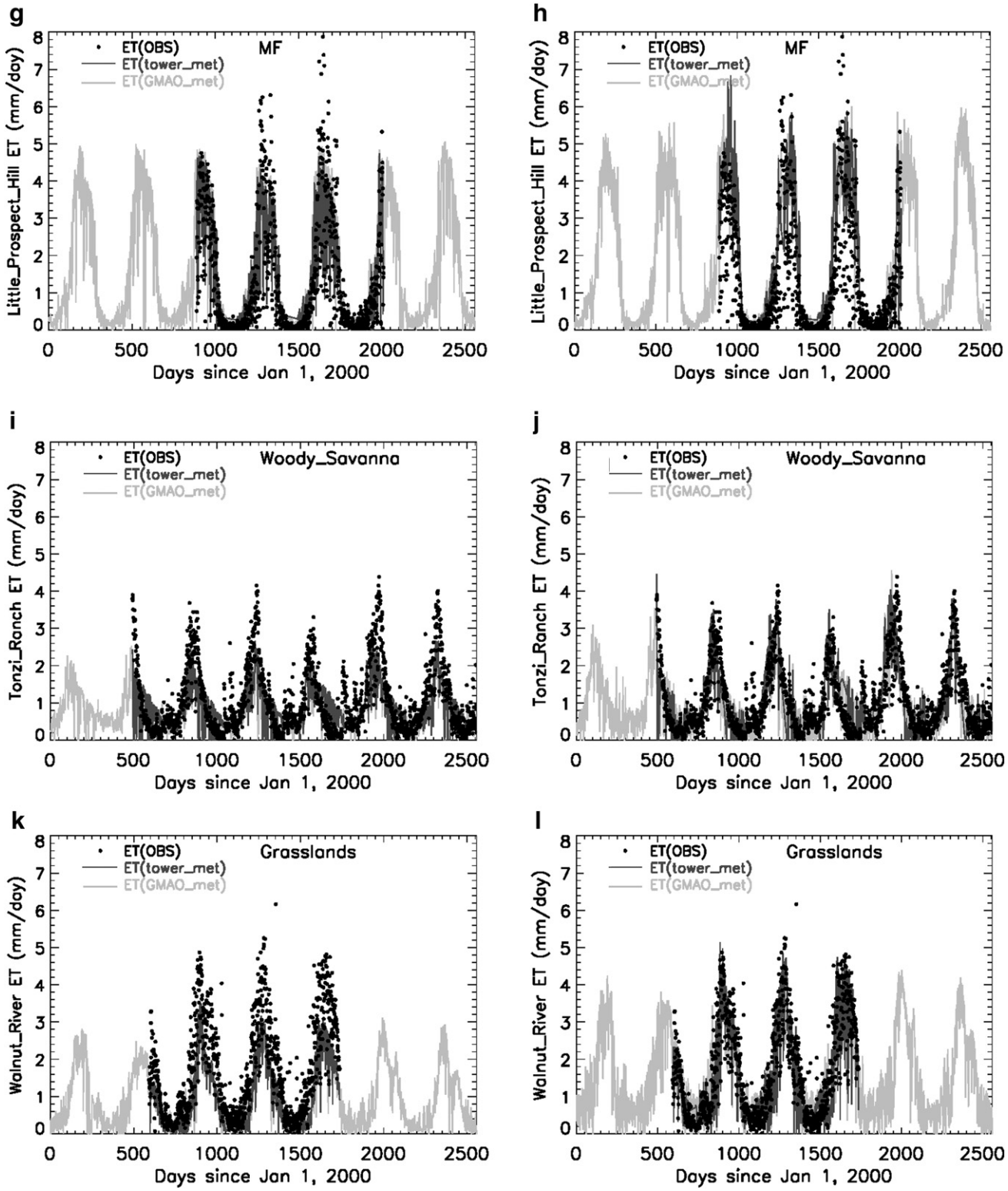

Fig. 6 (*continued*).

covariance ET measurements at three semiarid ecosystems, and found that eddy covariance towers usually underestimated the ET at high values and overestimated the ET at the low values.

3) Scaling from tower to landscape. The measuring height and the horizontal scale of measurement of the turbulent fluxes like latent heat fluxes and sensible heat fluxes, usually 2–5 m, have significant influences on the footprint (Schmid, 1997) and the size of underlying surface (Foken, 2008). Also, the complex terrain (Aubinet et al., 2005; Feigenwinter et al., 2008) and complicated canopy structure, the stochastic nature of turbulence (Hollinger & Richardson, 2005; Moncrieff et al., 1996) can affect the eddy covariance measurements (Yi, 2008; Yi et al., 2010). The comparison of measured ET with the estimated from the 3×3 1-km^2 MODIS across all 46 sites may introduce uncertainties due

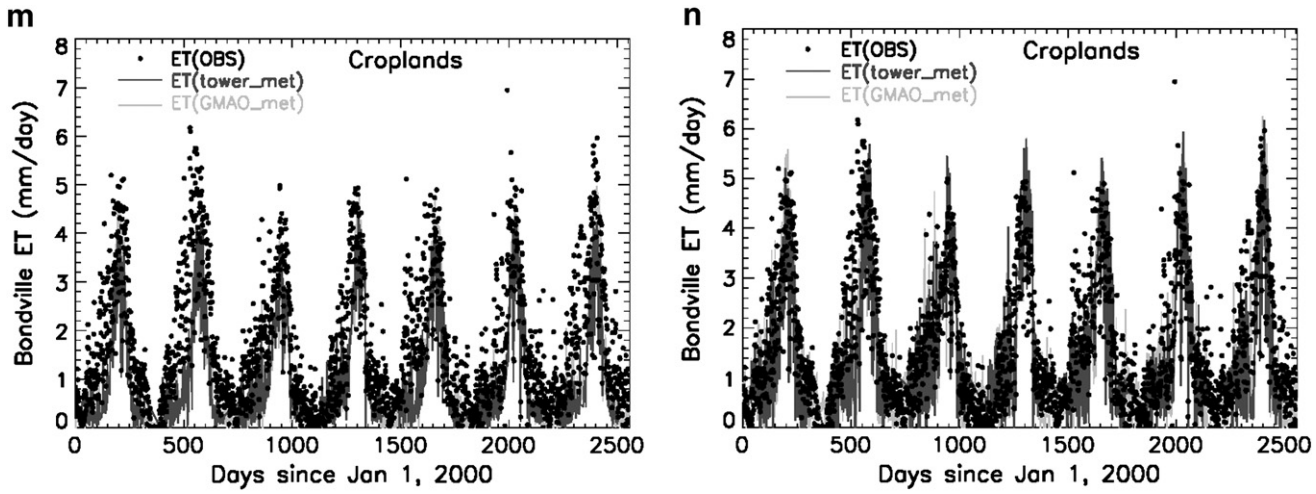

Fig. 6 (*continued*).

to the differences in tower footprints for different towers and under varying environmental conditions for a given tower. For example, among the 46 towers used to examine the performance of the ET algorithms, there are seven eddy covariance towers at MB, Canada (CANS1…7), which are very close and are all ENF (Table 4). The ET measurements at the seven CANS towers are quite different, with the average daily ET ranging from 0.38 to 0.59 mm day^{-1} (Table 4). The magnitudes and interannual variability substantially differ among the seven CANS towers. And in heterogeneous areas, the differing scales of the tower and MODIS ET estimates should be performed via an upscaling process, such as that used during the Bigfoot MODIS validation project (Cohen et al., 2003; Turner, et al., 2003a; Turner, et al., 2003b). The expense and intensity of such studies, however, limit our ability to perform such comparisons.

4) Algorithm limitations. A large number of physical factors are involved in soil surface evaporation and plant transpiration processes, including microclimate, plant biophysics for site specific species and landscape heterogeneity, making accurate assessment of ET a challenge (Friedl, 1996; McVicar et al., 2007; Vörösmarty, et al., 1998). Some issues remaining in the ET algorithm may contribute to the differences between the tower ET measurements and the ET estimates by the algorithm. The algorithm doesn't account for the stand age, disturbance history or species composition. Biophysical parameters such as *gl_sh*, rbl_{max} and rbl_{min}, VPD_{open} and VPD_{close} used in the algorithm have uncertainties since the same values are used for a given biome type globally. We have little knowledge regarding some parameters (e.g., the soil heat fluxes, the boundary layer resistance for soil evaporation) and the mechanisms involved. Although it is generally assumed that stomata close at night, several studies have documented nighttime stomatal opening in many species over a range of habitats (Musselman & Minnick, 2000). Incomplete stomatal closure during the night is observed in a diverse range of vegetation types (Caird et al., 2007; Daley & Phillips, 2006; Zeppel et al., 2010). Assumption of the stomata closure at night can induce biases to the nighttime plant transpiration, and hence induce underestimated daily total ET. Increasing CO_2 content tends to reduce plant transpiration due to a high-CO_2 induced partial stomatal closure (Idso & Brazel, 1984). Within one or two decades, this effect on ET may be negligible; however, as data record lengthens, this effect is needed to account for. As a result, theoretically, we may overestimate ET with time. We will add antitranspiration effect from enriched CO_2 to the transpiration module in our algorithm when we study the long-term remotely sensed ET changes.

7. Conclusions

We have improved the old ET algorithm by 1) simplifying the calculation of vegetation cover fraction (F_C); 2) calculating ET as the sum of daytime and nighttime components; 3) calculating soil heat flux; 4) improving the methods to estimate stomatal conductance, aerodynamic resistance and boundary layer resistance; 5) separating dry canopy surface from the wet, and hence canopy water loss includes evaporation from the wet canopy surface and transpiration from the dry surface; and 6) dividing soil surface into saturated wet surface and moist surface, and thus soil evaporation includes potential evaporation from the saturated wet surface and actual evaporation from the moist surface. Globally, calibrating BPLUT was based on the calculation of the WUE using the tower observed ET, GPP, and the MODIS GPP for each vegetation type; also the spatial pattern of the ET was checked with the global precipitation (Chen et al., 2002). Locally, the ET estimates were compared to tower ET measurements for calibration of parameters.

Both the old and the improved ET algorithms were applied globally with the GMAO and MODIS land cover, LAI/FPAR, albedo data. The total global annual ET over the vegetated land surface areas during 2000–2006, 62.8×10^3 km^3, estimated by the improved algorithm, agrees well with the reported ET of 65.5×10^3 km^3 over the terrestrial land surface by Oki and Kanae (2006). The improved global total ET is a little less than 65.5×10^3 km^3 reported by Oki and Kanae (2006) because the MODIS ET doesn't include urban and barren areas since there is no MODIS LAI/FPAR for these land cover types.

The performance of the improved ET algorithm was also examined at 46 AmeriFlux eddy covariance flux towers driven by two sets of meteorological data, tower measured meteorological data and global GMAO meteorological data. Results show that the improved algorithm enhances ET estimates, reducing the tower-specific MAE of the daily ET from 0.39 mm day^{-1} with the old algorithm to 0.33 mm day^{-1}, and reducing the GMAO-driven MAE from 0.40 mm day^{-1} to 0.31 mm day^{-1}, which means that the improved ET estimates capture the magnitudes of the ET measurements better than the old ones. MAE values are 24.6% and 24.1% of the ET measurements by the improved algorithm, within the 10–30% range of the accuracy of ET measurements (Courault et al., 2005; Jiang et al., 2004; Kalma et al., 2008). The correlation coefficients of the tower-specific improved ET estimates with the ET measurements averaged over all the available days increases from 0.83 with the old algorithm (Fig. 7a) to 0.86 (Fig. 7c), and from 0.81 (Fig. 7b) to 0.86 (Fig. 7d) driven by GMAO meteorological data. The contribution of average annual nighttime ET to annual total ET is 9.53% driven by the global GMAO

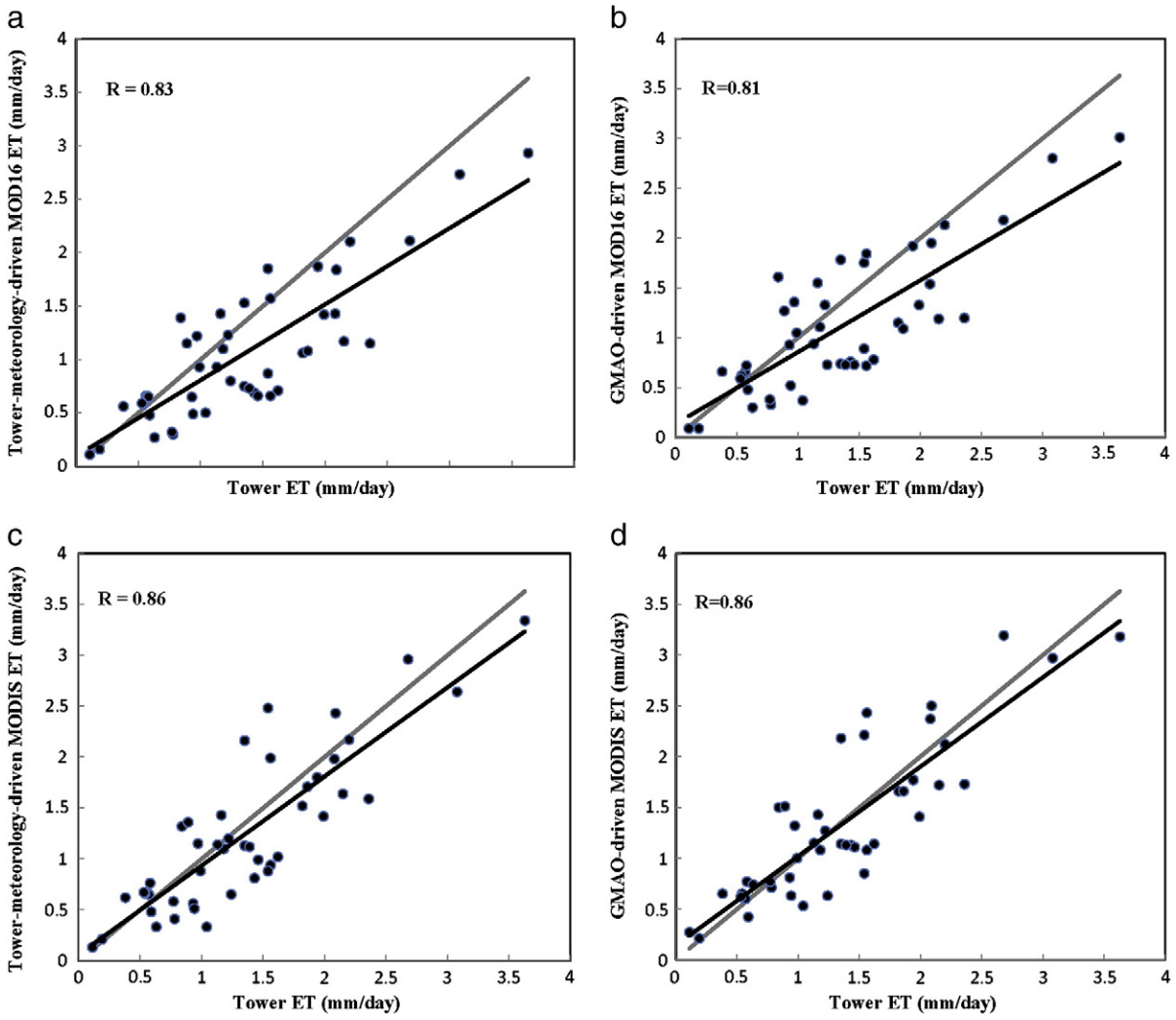

Fig. 7. Comparisons of the average ET observations to the average daily ET estimates with the old and the improved algorithms across all the available days at the 46 flux tower sites. These data were created using (1) tower-specific meteorology (a and c) and (2) the global GMAO meteorology (b and d) with the old (a and b) and the improved (c and d) MOD16 ET algorithms. The solid grey lines represent that the ratio of ET estimates to ET measurements is 1.0 and the solid black lines are the regression of the ET estimates to measurements.

meteorological data (Table 4), and the ratio of annual soil heat flux to annual LE driven by GMAO is substantial at some sites (Table 4), which means that the nighttime ET and soil heat flux should not be neglected. Based on those results, we conclude that the improved ET algorithm improves the generation of near-real-time, 8-day and annual ET products, providing critical information on global terrestrial water and energy cycles and environmental changes. More importantly, the improved MODIS ET products will provide information to land and water managers and policy makers to comprise the growing competition for the limited water supplies and to reduce the cost of irrigation projects (Teuling et al., 2009).

This MODIS ET algorithm will now be submitted to NASA for full Algorithm Theoretical Basis Document review. In the interim we will make this dataset available in a beta test mode to interested users by contacting the senior author. Once NASA authorizes this dataset, it will be placed in the MODIS Land product DAAC for permanent distribution, and the dataset will be updated through 2010.

Acknowledgements

This research was financially supported by the NASA Earth Observing System MODIS project (grant NNX08AG87A). Eddy covariance flux tower sites are part of both the AmeriFlux and Fluxnet networks. We gratefully acknowledge the efforts of researchers at these sites and thank them for making their data available. Sites are funded through grants from the U.S. Department of Energy (DOE) Office of Biological and Environmental Research (BER) unless otherwise noted. Data collection at the ARM SGP Burn, ARM SGP Control and ARM SGP Main sites is supported by DOE of BER (contract number DE-AC02-05CH11231) as part of the Atmospheric Radiation Measurement Program, and at Bartlett AmeriFlux site funded by the USDA Forest Service, NASA, and DOE through the Northeastern Regional Center of the National Institute for Climate Change Research. Data collection and research is led by W. Oechel at Atqasuk, Ivotuk and Sky Oaks Old sites (funded by National Science Foundation), by T. Meyers at the Audubon Research Ranch, Bondville and Fort Peck sites, by A. Goldstein at Blodgett Research site, by T. Martin at the Donaldson site, by T. Kolb, S. Dore and M. Montes-Helu at Flagstaff Unmanaged Forest and Flagstaff Wildfire sites (supported by USDA CREES NRI 2004-35111-15057 and USDA NRI 2008-35101-19076), by K. Clark at the Fort Dix site (funded by USFS), by M. Litvak at Freeman Ranch Mesquite Juniper site, by T. Griffis and J. Baker at Rosemount G19 Alternative Management Corn Soybean Rotation and Rosemount G21 Conventional Management Corn Soybean Rotation, by R. Scott at Kendall Grassland site, by S. Saleska, J. W. Munger,

S. Wofsy and L. Hutyra at LBA Tapajos KM67 Mature Forest (funded by NASA), by H. da Rocha, M. Goulden and S. Miller at LBA Tapajos KM83 Logged Forest, by J. Hadley at Little Prospect Hill site, S. Verma at Mead Irrigated, Mead Irrigated Rotation and Mead Rainfed sites, by B. Law at Metolius New Young Pine, Metolius First Young Pine and Metolius Intermediate Pine sites (funded by the Office of Science (BER), DOE (Grant no. DE-FG02-06ER64318)), by L. Gu at Missouri Ozark site, by D. Dragoni at Morgan Monroe State Forest site, by R. K. Monson at Niwot Ridge site, by J. Chen at Ohio Oak Openings and Wisconsin Mature Red Pine sites, by A. Desai, P. Bolstad and B. Cook at Sylvania Wilderness site (funded by Office of Science (BER), DOE Terrestrial Carbon Processes program, grant number DE-FG02-00ER63023), by D. Baldocchi at Tonzi Ranch site, by P. Curtis at UMBS, by M. Goulden at UCI 1850, UCI 1930, UCI 1964, UCI 1964wet, UCI 1981, UCI 1989, UCI 1998 sites, by R. Coulter at Walnut River site, by K. Bible at Wind River Crane site, by K. Davis at Willow Creek (funded by the DOE's National Institute for Global Environmental Change program (NIGEC), and is currently supported by USDA-FS joint venture agreement 09-JV-11242306-105 and Wisconsin Focus on Energy under A. Desai at U. Wisconsin).

References

Allen, R. G., Tasumi, M., Morse, A., Trezza, R., Wright, J. L., Bastiaanssen, W., et al. (2007). Satellite-based energy balance for Mapping Evapotranspiration with Internalized Calibration (METRIC)—Applications.*Journal of Irrigation and Drainage Engineering*, *133*(4), 395 doi:10.1061(ASCE)0733-9437.

Anthoni, P. M., Unsworth, M. H., Law, B. E., Irvine, J., Baldocchi, D., & Moore, D. (2002). Seasonal differences in carbon and water vapor exchange in young and old-growth ponderosa pine ecosystems. *Agricultural and Forest Meteorology*, *111*, 203—222.

Aubinet, M. (2000). Estimates of the annual net carbon and water exchange of forests: The EUROFLUX methodology. *Advances in Ecological Research*, *30*, 113—175.

Aubinet, M., Berbigier, P., Bernhofer, C., et al. (2005). Comparing CO_2 storage and advection conditions at night at different CARBOEUROFLUX sites. *Boundary-Layer Meteorology*, *116*(1), 63—93.

Baldocchi, D. D. (2008). "Breathing" of the terrestrial biosphere: Lessons learned from a global network of carbon dioxide flux measurement systems. *Australian Journal of Botany*, *56*, 1—26.

Baldocchi, D. D., Xu, L., & Kiang, N. (2004). How plant functional-type, weather, seasonal drought, and soil physical properties alter water and energy fluxes of an oak-grass savanna and an annual grassland. *Agricultural and Forest Meteorology*, *123*(1–2), 13—39.

Bastiaanssen, W. G. M., Menenti, M., Feddes, R. A., & Holtslag, A. A. M. (1998a). The surface energy balance algorithm for land (SEBAL): Part 2 validation. *Journal of Hydrology*, *212–213*, 213—229.

Bastiaanssen, W. G. M., Menenti, M., Feddes, R. A., & Holtslag, A. A. M. (1998b). A remote sensing surface energy balance algorithm for land (SEBAL): 1. Formulation. *Journal of Hydrology*, *212–213*, 198—212.

Bastiaanssen, W. G. M., Noordman, E. J. M., Pelgrum, H., Davids, G., Thoreson, B. P., & Allen, R. G. (2005). SEBAL model with remotely sensed data to improve water-resources management under actual field conditions. *J Irrig Drain*, *131*, 85—93.

Bouchet, R. J. (1963). Evapotranspiration re'elle evapotranspiration potentielle, signification climatique. *International Association of Scientific Hydrology. Evaporation, vol. 2*. (pp. 134—142) Berkeley, Calif: General Assembly of Berkeley, Transactions.

Caird, M. A., Caird, J. H., & Caird, L. A. (2007). Nighttime stomatal conductance and transpiration in C3 and C4 plants. *Plant Physiology*, *143*, 4—10.

Chen, M., Xie, P., Janowiak, J. E., & Arkin, P. A. (2002). Global land precipitation: A 50-yr monthly analysis based on gauge observations. *Journal of Hydrometeorology*, *3*, 249—266.

Choudhury, B. J., & DiGirolamo, N. E. (1998). A biophysical process-based estimate of global land surface evaporation using satellite and ancillary data I. Model description and comparison with observations. *Journal of Hydrology*, *205*, 164—185.

Clark, K. L., Gholz, H. L., & Castro, M. S. (2004). Carbon dynamics along a chronosequence of slash pine plantations in north Florida. *Ecological Applications*, *14*, 1154—1171.

Cleugh, H. A., Leuning, R., Mu, Q., & Running, S. W. (2007). Regional evaporation estimates from flux tower and MODIS satellite data. *Remote Sensing of Environment*, *106*, 285—304.

Clothier, B. E., Clawson, K. L., Pinter, P. J., Jr., Moran, M. S., Reginato, R. J., & Jackson, R. D. (1986). Estimation of soil heat flux from net radiation during growth of al~:alfa. *Agricultural and Forest Meteorology*, *37*, 319—329.

Cohen, W. B., Maiersperger, T. K., Yang, Z., Gower, S. T., Turner, D. P., Ritts, W. D., et al. (2003). Comparisons of land cover and LAI estimates derived from ETM+ and MODIS for four sites in North America: A quality assessment of 2000/2001 provisional MODIS products. *Remote Sensing of Environment*, *88*, 233—255.

Cook, B. D., Davis, K. J., Wang, W., Desai, A., Berger, B. W., Teclaw, R. M., et al. (2004). Carbon exchange and venting anomalies in an upland deciduous forest in northern Wisconsin, USA. *Agricultural and Forest Meteorology*, *126*, 271—295.

Courault, D., Sequin, B., & Olioso, A. (2005). Review on estimation of evapotranspiration from remote sensing data: From empirical to numerical modeling approaches. *Irrigation and Drainage Systems*, *19*, 223—249.

da Rocha, H. R., Goulden, M. L., Miller, S. D., Menton, M. C., Pinto, L. D. V. O., de Freitas, H. C., et al. (2004). Seasonality of water and heat fluxes over a tropical forest in eastern Amazonia.*Ecological Applications*, *14*, 22—32 sp4.

Daley, M. J., & Phillips, N. G. (2006). Interspecific variation in nighttime transpiration and stomatal conductance in a mixed New England deciduous forest. *Tree Physiology*, *26*, 411—419.

Daughtry, C. S. T., Kustas, W. P., Moran, M. S., Pinter, P. J., Jr., Jackson, R. D., Brown, P. W., et al. (1990). Spectral estimates of net radiation and soil heat flux. *Remote Sensing of Environment*, *32*, 111—124.

Dawson, T. E., Burgess, S. S., Tu, K. P., Oliveira, R. S., Santiago, L. S., Fisher, J. B., et al. (2007). Nighttime transpiration in woody plants from contrasting ecosystems. *Tree Physiology*, *27*(4), 561—575.

Demarty, J., Chevallier, F., Friend, A. D., Viovy, N., Piao, S., & Ciais, P. (2007). Assimilation of global MODIS leaf area index retrievals within a terrestrial biosphere model. *Geophysical Research Letters*, *34*, L15402.

Desai, A. R., Bolstad, P. V., Cook, B. D., Davis, K. J., & Carey, E. V. (2005). Comparing net ecosystem exchange of carbon dioxide between an old-growth and mature forest in the upper Midwest, USA. *Agricultural and Forest Meteorology*, *128*(1–2), 33—55.

Engstrom, R., Hope, A., Kwon, H., Harazono, Y., Mano, M., & Oechel, W. (2006). Modeling evapotranspiration in Arctic coastal plain ecosystems using a modified BIOME-BGC model. *Journal of Geophysical Research*, *111*, G02021.

Feigenwinter, C., Bernhofe, C., Eichelmann, U., et al. (2008). Comparison of horizontal and vertical advective CO_2 fluxes at three forest sites. *Agricultural and Forest Meteorology*, *148*(1), 12—24.

Fisher, J. B., DeBiase, T. A., Qi, Y., Xu, M., & Goldstein, A. H. (2005). Evapotranspiration models compared on a Sierra Nevada forest ecosystem. *Environmental Modelling and Software*, *20*, 783—796.

Fisher, Malhi, J. Y., Bonal, D., da Rocha, H. R., de Araújo, A., Gamo, M., et al. (2009). The land–atmosphere water flux in the tropics. *Global Change Biology*, *15*(11), 2694—2714.

Fisher, J. B., Tu, K., & Baldocchi, D. D. (2008). Global estimates of the land atmosphere water flux based on monthly AVHRR and ISLSCP-II data, validated at FLUXNET sites. *Remote Sensing of Environment*, *112*(3), 901—919.

Foken, T. (2008). The energy balance closure problem: An overview. *Ecological Applications*, *18*(6), 1351—1367.

Friedl, M. A. (1996). Relationships among remotely sensed data, surface energy balance, and area-averaged fluxes over partially vegetated land surfaces. *Journal of Applied Meteorology*, *35*, 2091—2103.

Friedl, M. A., McIver, D. K., Hodges, J. C. F., Zhang, X. Y., Muchoney, D., Strahler, A. H., et al. (2002). Global land cover mapping from MODIS: Algorithms and early results. *Remote Sensing of Environment*, *83*(1–2), 287—302.

Gavilána, P., Berengena, J., & Allen, R. G. (2007). Measuring versus estimating net radiation and soil heat flux: Impact on Penman–Monteith reference ET estimates in semiarid regions. *Agricultural Water Management*, *89*, 275—286.

Gholz, H. L., & Clark, K. L. (2002). Energy exchange across a chronosequence of slash pine forests in Florida. *Agricultural and Forest Meteorology*, *112*, 87—102.

Glenn, E. P., Huete, A. R., Nagler, P. L., K.K., & Brown, P. (2007). Integrating remote sensing and ground methods to estimate evapotranspiration. *Critical Reviews in Plant Sciences*, *26*(3), 139—168.

Glenn, E. P., Huete, A. R., Nagler, P. L., & Nelson, S. G. (2008a). Relationship between remotely-sensed vegetation indices, canopy attributes and plant physiological processes: What vegetation indices can and cannot tell us about the landscape. *Sensors*, *8*, 2136—2160.

Glenn, E. P., Morino, K., Didan, K., Jordan, F., Carroll, K. C., Nagler, P. L., et al. (2008b). Scaling sap flux measurements of grazed and ungrazed shrub communities with fine and coarse-resolution remote sensing. *Ecohydrology*, *1*(4), 316—329.

Global Modeling and Assimilation Office (2004). File specification for GEOSDAS gridded output version 5.3, report. Greenbelt, Md: NASA Goddard Space Flight Cent.

Gowda, P. H., Chavez, J. L., Colaizzi, P. D., Evett, S. R., Howell, T. A., & Tolk, J. A. (2008). ET mapping for agricultural water management: present status and challenges. *Irrigation Science*, *26*, 223—237.

Hadley, J. L., Kuzeja, P. S., Daley, M. J., Phillips, N. G., Singh, S., & Mulcahy, T. (2008). Water use and carbon exchange of eastern hemlock (*Tsuga canadensis* L.) and deciduous forests in the northeastern U.S.: Implications for ecosystem-level effects of the hemlock woolly adelgid. *Tree Physiology*, *28*, 615—627.

Harazono, Y., Yoshimoto, M., Miyata, A., Uchida, Y., Vourlitis, G. L., & Oechel, W. C. (1995). *Micrometeorological data and their characteristics over the Arctic Tundra at Barrow, Alaska during the summer of 1993.Miscellaneous publication of the National Institute of Agro-Environmental Sciences No. 16, Japan* 213 pp.

Heinsch, F. A., Zhao, M., Running, S. W., Kimball, J. S., Nemani, R. R., Davis, K. J., et al. (2006). Evaluation of remote sensing based terrestrial productivity from MODIS using AmeriFlux tower eddy flux network observations. *IEEE Transactions on Geoscience and Remote Sensing*, *44*(7), 1908—1925.

Hill, M. J., Senarath, U., Lee, A., Zeppel, M., Nightingale, J. M., Williams, R. T., et al. (2006). Assessment of the MODIS LAI product for Australian ecosystems. *Remote Sensing of Environment*, *101*, 495—518.

Hollinger, D. Y., & Richardson, A. D. (2005). Uncertainty in eddy covariance measurements and its application to physiological models. *Tree Physiology*, *25*, 873—885.

Hope, A. S., Engstrom, R., & Stow, D. A. (2005). Relationship between AVHRR surface temperature and NDVI in arctic tundra ecosystems. *International Journal of Remote Sensing*, *26*(8), 1771—1776.

Huete, A., Didan, K., Miura, T., Rodriguez, E. P., Gao, X., & Ferreira, L. G. (2002). Overview of the radiometric and biophysical performance of the MODIS vegetation indices. *Remote Sensing of Environment*, *83*, 195−213.

Hutyra, L. R., Munger, J. W., Saleska, S. R., Gottlieb, E., Daube, B. C., Dunn, A. L., et al. (2007). Seasonal controls on the exchange of carbon and water in an Amazonian rainforest. *Journal of Geophysical Research*, *112*, G03008.

Idso, S. B., & Brazel, A. J. (1984). Rising atmospheric carbon dioxide concentrations may increase streamflow. *Nature*, *312*, 51−53.

Jacobsen, A., & Hansen, B. U. (1999). Estimation of the soil heat flux/net radiation ratio based on spectral vegetation indexes in high-latitude Arctic areas. *International Journal of Remote Sensing*, *20*(2), 445−461.

Jenkins, J. P., Richardson, A. D., Braswell, B. H., Ollinger, S. V., Hollinger, D. Y., & Smith, M. L. (2007). Refining light-use efficiency calculations for a deciduous forest canopy using simultaneous tower-based carbon flux and radiometric measurements. *Agricultural and Forest Meteorology*, *143*(1–2), 64−79.

Jiang, L., Islam, S., & Carlson, T. (2004). Uncertainties in latent heat flux measurement and estimation: Implications for using a simplified approach with remote sensing data. *Canadian Journal of Remote Sensing*, *30*, 769−787.

Jin, Y., Schaaf, C. B., Woodcock, C. E., Gao, F., Li, X., Strahler, A. H., et al. (2003). Consistency of MODIS surface BRDF/Albedo retrievals: 1. Algorithm performance. *Journal of Geophysical Research*, *108*(D5), 4158.

Jones, H. G. (1992). Plants and microclimate: A quantitative approach to environmental plant physiology. Cambridge, UK: Cambridge University Press.

Jung, M., Reichstein, M., Ciais, P., Seneviratne, S. I., Sheffield, J., Goulden, M. L., et al. (2010). Recent decline in the global land evapotranspiration trend due to limited moisture supply. *Nature*, *467*, 951−954.

Justice, C. O., Townshend, J. R. G., Vermote, E. F., Masuoka, E., Wolfe, R. E., Saleous, N., et al. (2002). An overview of MODIS Land data processing and product status. *Remote Sensing of Environment*, *83*, 3−15.

Kalma, J. D., McVicar, T. R., & McCabe, M. F. (2008). Estimating land surface evaporation: A review of methods using remotely sensed surface temperature data. *Surveys in Geophysics*, *29*, 421−469.

Kelliher, F. M., Leuning, R., Raupach, M. R., & Schulze, E. D. (1995). Maximum conductances for evaporation from global vegetation types. *Agricultural and Forest Meteorology*, *73*(1–2), 1−16.

Korzoun, V. I., Sokolov, A. A., Budyko, M. I., Voskresensky, K. P., & Kalinin, G. P. (1978). World water balance and water resources of the earth (English). *Studies and Reports in Hydrology (UNESCO), no. 25/United Nations Educational, Scientific and Cultural Organization, 75 - Paris (France); International Hydrological Decade*. Moscow (USSR): USSR National Committee 663 p.

Kustas, W., & Anderson, M. (2009). Advances in thermal infrared remote sensing for land surface modeling. *Agricultural and Forest Meteorology*, *149*, 2071−2081.

Kustas, W. P., & Daughtry, C. S. T. (1990). Estimation of the soil heat flux/net radiation ratio from spectral data. *Agricultural and Forest Meteorology*, *49*, 205−223.

Landsberg, J. J., & Gower, S. T. (1997). Applications of physiological ecology to forest management. : Academic Press.

Law, B. E., Falge, E., Gu, L., Baldocchi, D. D., Bakwin, P., Berbigier, P., et al. (2002). Environmental controls over carbon dioxide and water vapor exchange of terrestrial vegetation. *Agricultural and Forest Meteorology*, *113*(1–4), 97−120.

Liski, J., Nissinen, A., Erhard, M., & Taskinen, O. (2003). Climatic effects on litter decomposition from Arctic tundra to tropical rainforest. *Global Change Biology*, *9*(4), 575−584.

Los, S. O., Collatz, G. J., Sellers, P. J., Malmstrom, C. M., Pollack, N. H., DeFries, R. S., et al. (2000). A global 9-yr biophysical land surface dataset from NOAA AVHRR data. *Journal of Hydrometeorology*, *1*(2), 183−199.

L'vovich, M. I., & White, G. F. (1990). Use and transformation of terrestrial water systems. In B. L. TurnerII, W. C. Clark, R. W. Kates, J. F. Richards, J. T. Mathews, & W. B. Meyer (Eds.), *The Earth as transformed by human action* (pp. 235−252). Cambridge, UK: Cambridge University Press.

Maidment, D. R. (1993). Handbook of hydrology: McGraw-Hill. ISBN: 0070397325/9780070397323.

McVicar, T. R., Van Niel, T. G., Li, L., King, E. A., & Donohue, R. J. (2007). *Deriving moisture availability from time series remote sensing for ecohydrological applications: Development of a prototype near real-time operational system.* CSIRO Land and Water Science Report 37/07.

Mellouli, H. J., van Wesemael, B., Poesen, J., & Hartmann, R. (2000). Evaporation losses from bare soils as influenced by cultivation techniques in semi-arid regions. *Agricultural Water Management*, *42*(3), 355−369.

Moncrieff, J. B., Malhi, Y., & Leuning, R. (1996). The propagation of errors in long-term measurements of land-atmosphere fluxes of carbon and water. *Global Change Biology*, *2*(3), 231−240.

Monteith, J. L. (1965). Evaporation and environment. *Symposium of the society of experimental biology*, *19*, 205−224.

Mu, Q., Heinsch, F. A., Zhao, M., & Running, S. W. (2007a). Development of a global evapotranspiration algorithm based on MODIS and global meteorology data. *Remote Sensing of Environment*, *111*, 519−536.

Mu, Q., Zhao, M., Heinsch, F. A., Liu, M., Tian, H., & Running, S. W. (2007b). Evaluating water stress controls on primary production in biogeochemical and remote sensing based models. *Journal of Geophysical Research*, *112*, G01012.

Musselman, R. C., & Minnick, T. J. (2000). Nocturnal stomatal conductance and ambient air quality standards for ozone. *Atmospheric Environment*, *34*, 719−733.

Myneni, R. B., Hoffman, S., Knyazikhin, Y., Privette, J. L., Glassy, J., Tian, Y., et al. (2002). Global products of vegetation leaf area and fraction absorbed PAR from year one of MODIS data. *Remote Sensing of Environment*, *83*(1–2), 214−231.

Nagler, P., Cleverly, J., Lampkin, D., Glenn, E., Huete, A., & Wan, Z. (2005). Predicting riparian evapotranspiration from MODIS vegetation indices and meteorological data. *Remote Sensing of Environment*, *94*, 17−30.

Nishida, K., Nemani, R., Glassy, J. M., & Running, S. W. (2003). Development of an evapotranspiration index from Aqua/MODIS for monitoring surface moisture status. *IEEE Transactions on Geoscience and Remote Sensing*, *41*(2).

Ogée, J., Lamaud, E., Brunet, Y., Berbigier, P., & Bonnefond, J. M. (2001). A long-term study of soil heat flux under a forest canopy. *Agricultural and Forest Meteorology*, *106*(3), 173−186.

Oki, T., & Kanae, S. (2006). Global hydrological cycles and world water resources. *Science*, *313*(5790), 1068−1072.

Overgaard, J., Rosbjereg, D., & Butts, M. (2006). Land-surface modeling in hydrological perspective — A review. *Biogeosciences*, *3*, 229−241.

Priestley, C. H. B., & Taylor, R. J. (1972). On the assessment of surface heat flux and evaporation using large scale parameters. *Monthly Weather Review*, *100*, 81−92.

Rocha, H. R., Manzi, A. O., Cabral, O., Miller, S., Goulden, M., Saleska, S., et al. (2009). Patterns of water and heat flux across a biome gradient from tropical forest to savanna in Brazil. *Journal of Geophysical Research – Biogeosciences*, *114*, G00B12.

Rosegrant, M. W., Cai, X., & Cline, S. A. (2003). Will the world run dry? Global water and food security. *Environment: Where Science and Policy Meet*, *45*(7).

Running, S. W., & Kimball, J. S. (2005). Satellite-based analysis of ecological controls for land-surface evaporation resistance. In M. Anderson (Ed.), *Encyclopedia of hydrological sciences*. : John Wiley & Sons, Ltd 2005.

Running, S. W., Nemani, R. R., Heinsch, F. A., Zhao, M., Reeves, M. C., & Hashimoto, H. (2004). A continuous satellite-derived measure of global terrestrial primary production. *Bioscience*, *54*, 547−560.

Salomon, J., Schaaf, C. B., Strahler, A. H., Gao, F., & Jin, Y. (2006). Validation of the MODIS bidirectional reflectance distribution function and albedo retrievals using combined observations from the aqua and terra platforms. *IEEE Transactions on Geoscience and Remote Sensing*, *44*(6), 1555−1565.

Schaaf, C. B., Gao, F., Strahler, A. H., Lucht, W., Li, X., Tsang, T., et al. (2002). First operational BRDF, albedo and nadir reflectance products from MODIS. *Remote Sensing of Environment*, *83*, 135−148.

Schmid, H. P. (1997). Experimental design for flux measurements: Matching scales of observations and fluxes. *Agricultural and Forest Meteorology*, *87*, 179−200.

Schulze, E. -D., Kelliher, F. M., Körner, C., Lloyd, J., & Leuning, R. (1994). Relationships among maximum stomatal conductance, ecosystem surface conductance, carbon assimilation rate and plant nitrogen nutrition: A global ecology scaling exercise. *Annual Review of Ecology and Systematics*, *25*, 629−660.

Scott, R. L. (2010). Using watershed water balance to evaluate the accuracy of eddy covariance evaporation measurements for three semiarid ecosystems. *Using watershed water balance to evaluate the accuracy of eddy covariance evaporation measurements for three semiarid ecosystems. Agricultural and Forest Meteorology*, *150*, 219−225.

Shuttleworth, W. J. (2007). Putting the "vap" into evaporation. *Hydrology and Earth System Sciences*, *11*, 210−244.

Stewart, J. B., Kustus, W. P., Humes, K. S., Nichols, W. D., Moran, M. S., & De Bruin, H. A. R. (1994). Sensible heat flux–radiometric surface temperature relationship for eight semiarid areas. *Journal of Applied Meteorology*, *33*, 1110−1117.

Su, Z. (2002). The surface energy balance system (SEBS) (for estimation of turbulent heat fluxes). *Hydrology and Earth System Sciences*, *6*, 85−99.

Tanaka, N., Kume, T., Yoshifuji, N., Tanaka, K., Takizawa, H., Shiraki, K., et al. (2008). A review of evapotranspiration estimates from tropical forests in Thailand and adjacent regions. *Agricultural and Forest Meteorology*, *148*, 807−819.

Taylor, K. E. (2001). Summarizing multiple aspects of model performance in a single diagram. *Journal of Geophysical Research*, *106*, 7183−7192.

Teuling, A. J., Hirschi, M., Ohmura, A., Wild, M., Reichstein, M., Ciasis, P., et al. (2009). A regional perspective on trends in continental evaporation. *Geophysical Research Letters*, *36*, L02404.

Thomas, C. K., Law, B. E., Irvine, J., Martin, J. G., Pettijohn, J. C., & Davis, K. J. (2009). Seasonal hydrology explains interannual and seasonal variation in carbon and water exchange in a semi-arid mature ponderosa pine forest in Central Oregon. *Journal of Geophysical Research*, *114*, G04006.

Thornton, P.E. (1998) Regional ecosystem simulation: combining surface- and satellite-based observations to study linkages between terrestrial energy and mass budgets. PhD. Dissertation, School of Forestry, The University of Montana, Missoula, MT., 280 pp.

Trenberth, K. E., Fasullo, J., & Kiehl, J. (2009). Earth's global energy budget. *Bulletin of the American Meteorological Society*, *90*(3), 311−323.

Turner, D. P., Ritts, W. D., Cohen, W. B., Gower, S. T., Zhao, M., Running, S. W., et al. (2003a). Scaling gross primary production (GPP) over boreal and deciduous forest landscapes in support of MODIS GPP product validation. *Remote Sensing of Environment*, *88*, 256−270.

Turner, D. P., Urbanski, S., Bremer, D., Wofsy, S. C., Meyers, T., Gower, S. T., et al. (2003b). A cross-biome comparison of daily light use efficiency for gross primary production. *Global Change Biology*, *9*, 383−395.

Van de Griend, A. A. (1994). Bare soil surface resistance to evaporation by vapor diffusion under semiarid conditions. *Water Resources Research*, *30*, 181−188.

Vickers, D., Gockede, M., & Law, B. (2010). Uncertainty estimates for 1-hour averaged turbulence fluxes of carbon dioxide, latent heat and sensible heat. *Tellus B*, *62*, 87−99.

Vörösmarty, C. J., Federer, C. A., & Schloss, A. L. (1998). Potential evaporation function compared on US watersheds: Possible implication for global-scale water balance and terrestrial ecosystem. *Journal of Hydrology*, *207*, 147−169.

Vörösmarty, C. J., McIntyre, P. B., Gessner, M. O., Dudgeon, D., Prusevich, A., Green, P., et al. (2010). Global threats to human water security and river biodiversity. *Nature*, *467*, 555−561.

Wallace, J. S., & Holwill, C. J. (1997). Soil evaporation from tiger-bush in south-west Niger. *Journal of Hydrology*, *188–189*, 426−442.

Wang, Y., Woodcock, C. E., Buermann, W., Sternberg, P., Voipoi, P., Smolander, H., et al. (2004). Evaluation of the MODIS LAI algorithm at a coniferous forest site in Finland. *Remote Sensing of Environment*, *91*, 114−127.

Weber, S., Graf, A., & Heusinkveld, B. G. (2007). Accuracy of soil heat flux plate measurements in coarse substrates — Field measurements versus a laboratory test. *Theoretical and Applied Climatology*, *89*(39479), 109−114.

White, M. A., Thornton, P. E., Running, S. W., & Nemani, R. R. (2000). Parameterization and sensitivity analysis of the BIOME-BGC terrestrial ecosystem model: Net primary production controls. *Earth Interactions*, *4*(3), 1−85.

Wilson, K., Goldstein, A., Falge, E., Aubinet, M., Baldocchi, D., Berbigier, P., et al. (2002). Energy balance closure at FLUXNET sites. *Agricultural and Forest Meteorology*, *113*, 223−243.

Xu, L., & Baldocchi, D. D. (2003). Seasonal trend of photosynthetic parameters and stomatal conductance of blue oak (*Quercus douglasii*) under prolonged summer drought and high temperature. *Tree Physiology*, *23*, 865−877.

Yang, W., Tan, B., Huang, D., Rautiainen, M., Shabanov, N. V., Wang, Y., et al. (2006). MODIS leaf area index products: From validation to algorithm improvement. *IEEE Transactions on Geoscience and Remote Sensing*, *44*, 1885−1898.

Yi, C. (2008). Momentum transfer within canopies. *Journal of Applied Meteorology and Climatology*, *47*(1), 262−275.

Yi, C., Ricciuto, D., Li, R., Xu, X., et al. (2010). Climate control of terrestrial carbon exchange across biomes and continents. *Environmental Research Letters*, 5.

Yuan, W. P., Liu, S. G., Yu, G. R., Bonnefond, J. M., Chen, J. Q., Davis, K., et al. (2010). Global estimates of evapotranspiration and gross primary production based on MODIS and global meteorology data. *Remote Sensing of Environment*, *114*(7), 1416−1431.

Zeppel, M., Tissue, D., Taylor, D., Macinnis-NG, C., & Eamus, D. (2010). Rates of nocturnal transpiration in two evergreen temperate woodland species with differing water-use strategies. *Tree Physiology*, *30*, 988−1000.

Zhang, K., Kimball, J. S., Mu, Q., Jones, L. A., Goetz, S., & Running, S. W. (2009). Satellite based analysis of northern ET trends and associated changes in the regional water balance from 1983 to 2005. *Journal of Hydrology*, *379*, 92−110.

Zhao, M., Heinsch, F. A., Nemani, R., & Running, S. W. (2005). Improvements of the MODIS terrestrial gross and net primary production global data set. *Remote Sensing of Environment*, *95*, 164−176.

Zhao, M., & Running, S. W. (2010). Drought-induced reduction in global terrestrial net primary production from 2000 through 2009. *Science*, *329*, 940−943.

Zhao, M., Running, S. W., & Nemani, R. R. (2006). Sensitivity of moderate resolution imaging spectroradiometer (MODIS) terrestrial primary production to the accuracy of meteorological reanalyses. *Journal of Geophysical Research*, *111*, G01002.